

LOCKHEED MARTIN ENERGY RESEARCH LIBRARIES



3 4456 0515827 2

ORNL-4224

UC-80 - Reactor Technology

SIZE CLASSIFICATION OF SUBMICRON PARTICLES  
BY A LOW-PRESSURE CASCADE IMPACTOR

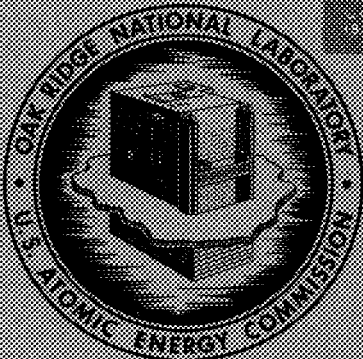
G. W. Parker  
H. Buchholz

OAK RIDGE NATIONAL LABORATORY  
CENTRAL RESEARCH DIVISION  
DOCUMENT COLLECTION

**LIBRARY LOAN COPY**

DO NOT TRANSFER TO ANOTHER PERSON

If you wish someone else to see this  
document, send it home with document  
and the library will arrange delivery.



**OAK RIDGE NATIONAL LABORATORY**  
operated by  
**UNION CARBIDE CORPORATION**  
for the  
**U. S. ATOMIC ENERGY COMMISSION**

-----  
LEGAL NOTICE

This report was prepared as an account of Government sponsored work. Neither the United States, nor the Commission, nor any person acting on behalf of the Commission:

- A. Makes any warranty or representation, expressed or implied, with respect to the accuracy, completeness, or usefulness of the information contained in this report, or that the use of any information, apparatus, method, or process disclosed in this report may not infringe privately owned rights; or
- B. Assumes any liabilities with respect to the use of, or for damages resulting from the use of any information, apparatus, method, or process disclosed in this report.

As used in the above, "person acting on behalf of the Commission" includes any employee or contractor of the Commission, or employee of such contractor, to the extent that such employee or contractor of the Commission, or employee of such contractor prepares, disseminates, or provides access to, any information pursuant to his employment or contract with the Commission, or his employment with such contractor.

-----

ORNL-4226

Contract No. W-7405-eng-26

REACTOR CHEMISTRY DIVISION

SIZE CLASSIFICATION OF SUBMICRON PARTICLES  
BY A LOW-PRESSURE CASCADE IMPACTOR

G. W. Parker

H. Buchholz

JUNE 1968

OAK RIDGE NATIONAL LABORATORY  
Oak Ridge, Tennessee  
Operated by  
UNION CARBIDE CORPORATION  
for the  
U.S. ATOMIC ENERGY COMMISSION

LOCKHEED MARTIN ENERGY RESEARCH LIBRARIES



3 4456 0515827 2



## CONTENTS

	PAGE
Abstract . . . . .	1
1. Introduction . . . . .	2
2. Theoretical Considerations . . . . .	2
3. Experimental Approach . . . . .	9
3.1 General Assembly . . . . .	9
3.2 Particle Generation . . . . .	11
3.3 Low-Pressure Cascade Impactor Mark I . . . . .	12
3.4 Low-Pressure Cascade Impactor Mark II . . . . .	16
3.5 Method of Analysis . . . . .	18
3.6 Containment Research Installation (CRI) Experiment . . . . .	19
4. Results and Discussion . . . . .	21
4.1 Experimental Verification of the High Retention of Small Particles in the Cascade Impactor Under Reduced Pressure . . . . .	21
4.2 Particle Loss . . . . .	22
4.2.1 Particle Loss on the Wall . . . . .	24
4.2.2 Particle Loss from the Impaction Plate . . . . .	26
4.3 Radioiodine and Radiocesium in the CRI, Analyzed by the Low-Pressure Cascade Impactor . . . . .	28
5. Summary . . . . .	33
6. Acknowledgment . . . . .	34
7. Appendix: Calibration of the Low-Pressure Cascade Impactors . . . . .	35
8. References . . . . .	40



# SIZE CLASSIFICATION OF SUBMICRON PARTICLES

BY A LOW-PRESSURE CASCADE IMPACTOR

G. W. Parker

H. Buchholz\*

## ABSTRACT

Aerosol particles in the submicron range are expected to be released as a consequence of a more or less severe core meltdown in a reactor accident. The behavior of aerosol particles is often explainable exclusively in terms of the laws of mechanics, which invariably include particle size as one parameter. Devices to measure particle size in the submicron region are therefore required; and a simple, passive, nearly foolproof device is particularly desirable.

The principle of the cascade impactor is simple. A gas which is carrying particles, is accelerated through a nozzle and impinged on a plate; particles having sufficient inertia (i.e. the large particles) leave the jet stream lines and settle on the plate. Successive stages with jets of increasing velocity remove successively smaller particles. Operation at low pressure increases the mean free path of the gas molecules and the Cunningham correction (for the slip of small particles between gas molecules). This enables one to design a cascade impactor of reasonable jet size which will separate submicron particles.

In this work a commercially available (Andersen) impactor, modified for low pressure operation, and an impactor of original design were built, tested and calibrated. Design data and calibration curves are reported. The particle size range separated is from about  $0.01 \mu$  to several microns diameter. The original design impactor is assembled and disassembled very simply and employs throw-away impactor plates to facilitate decontamination.

---

\* Present address: Hahn-Meitner-Institut Für Kernforschung, Berlin, Germany.

## 1. INTRODUCTION

Particles having a diameter of about  $0.1 \mu$  and less are highly retained in the respiratory tract,<sup>1</sup> and particles in this size range are expected to be released as a consequence of a more or less severe core meltdown in a reactor accident.<sup>2</sup> Large particles are removed quickly from the atmosphere by sedimentation whereas particles having a diameter less than  $1 \mu$  remain airborne long enough to constitute a hazard. The hazard is a consequence both of their high retention in the respiratory tract and their radioactivity.

Knowledge concerning the size distribution of particles released in simulated reactor accidents and the radioactive species carried by them is still lacking because suitable instruments to measure size distribution are not available. Predictions of the conditions in a real reactor accident are therefore unreliable.

A modified cascade impactor can provide some of the needed data. This device not only separates particles having different sizes, but also permits identification of the radioactive species which each size group is carrying. Impactors are ordinarily limited to particles larger than  $0.5 \mu$ , whereas particles of  $0.1 \mu$  and smaller are of interest in nuclear safety research. The efficiency of depositing smaller particles in an impactor can be improved by operating the impactor at low pressure.<sup>3,4</sup>

## 2. THEORETICAL CONSIDERATIONS

The basic theory of the impaction principle is quite simple. When a gas jet carrying particles is directed toward a surface, all particles having sufficient inertia leave their stream lines and settle on the surface. Smaller particles remain within the jet stream. In the next stage,

the gas passes through smaller holes and the jet is accelerated to a higher velocity. The probability of smaller particles settling is thus increased. This basic principle is demonstrated in Fig. 1.

It was first found by K. R. May<sup>5</sup> that the efficiency for depositing particles depends on a dimensionless term, called the impaction parameter, which is characteristic for each type of impactor. Efficiency curves were then calculated by W. E. Ranz and J. B. Wong<sup>6</sup> and by C. N. Davies and M. Aylward<sup>7</sup> for circular and rectangular jets in different geometrical arrangements. A plot of the efficiency versus impaction parameter always shows the characteristic S-shape. This theoretical relation is verified by experimental results. Using the relationship between impaction parameter and particle diameter, given in Eq. (1), one can calculate the efficiency for depositing a certain particle size from the efficiency curves.

$$\psi = \frac{C\rho D^2 v}{18\eta D_j} \quad (1)$$

$\psi$  = impaction parameter, dimensionless

C = Cunningham correction, correction for particles with sizes comparable to the mean free path of the gas molecules

$\rho$  = specific gravity of particles, g/cc

D = diameter of particles, cm

$\eta$  = viscosity of gas, poise

$D_j$  = diameter of jet, cm

v = velocity of jet, cm/sec.

The derivation of Eq. (1) is based on the following basic assumptions: spherical particles of negligible size, viscous gas flow, uniform velocity field and no bounce of particles. The efficiencies calculated are somewhat higher than observed.

If  $\psi$  approaches 1, the deposition efficiency will become 100%. On the other hand, if  $\psi = 0$ , the deposition efficiency is zero also. In the range between  $\psi = 1$  and  $\psi = 0$ , the efficiency increases continuously with  $\psi$  according to an S-shape characteristic. It is quite common to compare the performance of impactor stages by the diameter of particles deposited with a 50% efficiency. This diameter shall be called  $D_{50}$  or the stage constant and the corresponding impaction parameter  $\psi_{50}$ .

In search of ways to increase the efficiency of depositing submicron particles, Eq. (1) may be examined. Because  $\psi$  is replaced by  $\psi_{50}$ , a constant of the impactor stage, the right side of the equation also becomes constant. Therefore, three factors remain to influence the value of  $D_{50}$ . These are the Cunningham-Correction describing the slip of particles in the gas stream, the jet velocity and the jet diameter. In order to lower  $D_{50}$  beyond  $0.5 \mu$  by changing  $v$  and  $D_j$ , it would be necessary to exceed  $1/3$  of the velocity of sound or to drill holes smaller than 0.2 mm in diameter. But these values are practical limits; particles of velocity greater than  $1/3$  Mach bounce significantly and the deposition is lowered by an unknown factor.<sup>8</sup> In addition, the gas which enters the nozzle<sup>9</sup> expands adiabatically within the nozzle. Holes smaller than 0.2 mm are not only difficult to drill, especially the large number necessary to maintain the gas flow, but they also have the disadvantage of imposing significant pressure drops.

The applicability of the impaction theory at reduced pressure was verified by S. C. Stern et al.<sup>10</sup> taking into account the pressure dependence of the Cunningham-Correction in Eq. (1). Another proof was given by A. F. McFarland and H. W. Zeller,<sup>8</sup> in their experimental results of the ". . . Impactor for High Altitude." These findings indicate that the cascade impactor can be used to separate particles in the small size range of interest.

The Cunningham-Correction C, based on the work of R. A. Millikan<sup>11</sup> is defined according to Eq. (2).<sup>8,10</sup>

$$C = 1 + \frac{2\lambda}{D} \left( 1.23 + 0.41 e^{-0.44 D/\lambda} \right) \quad (2)$$

where  $\lambda$  is the mean free path of the gas molecules which constitute the gas phase and D is the diameter of the particles. In air:

$$C = 1 + \frac{10^{-2}}{pD} \left( 1.23 + 0.41 e^{-86pD} \right), \quad (2a)$$

where p is the air pressure (mm Hg) and the particle diameter, D, is in cm. C increases, if the mean free path of the gas molecules increases. C is larger for smaller particles. At atmospheric pressure, C is about equal to unity for particles larger than  $1 \mu$  (see Fig. 2). By decreasing the pressure, C can be readily increased by more than two orders of magnitude for the particle sizes of interest.  $D_{50}$  is decreased by more than one order of magnitude, because  $(C) \propto (D_{50}^2)$  is constant according to Eq. (1).

The correction Millikan applied was relatively small, because  $\lambda/D$  was smaller than 47, whereas in the device reported by McFarland and Zeller<sup>8</sup> reasonable results were also obtained for  $\lambda/D = 1000$ , which means that C was about 6000. Thus, the application of Eq. (2) is justified for high correction values, too. In the experiments reported here, C was always less than 1000.

The jet velocity at the nozzle outlet may be replaced by the gas flow Q into the nozzle, a function of the nozzle diameter  $\pi/4 D_j^2$  and the ratio of gas density at the inlet and outlet,  $\rho/\rho_o$ .

$$v = \frac{Q}{\frac{\pi}{4} D_j^2 \rho/\rho_o} . \quad (3)$$

If Q is replaced by the external gas flow  $Q_a$ , the ratio of external to internal pressure  $p_a/p$  and the number of nozzles N, Eq. (3) becomes,

$$v = \frac{p_a Q_a}{p \frac{\pi}{4} D_j^2 N \rho/\rho_o} . \quad (4)$$

Denoting  $p (\rho/\rho_o) = p_o$ , inserting (4) into (1) one obtains

$$\psi_{50} = \frac{C(p_o, D_{50}) \rho p_a Q_a D_{50}^2}{18\eta D_j^3 p_o \frac{\pi}{4} N} . \quad (5)$$

If  $p_o$  (mm Hg)  $\times D_{50}$  (cm)  $< 10^{-3}$ , C is approximately,

$$C \approx 3.3 \frac{\lambda}{D_{50}} \approx \frac{1.7 \times 10^{-2}}{p \text{ (mm Hg)} D_{50} \text{ (cm)}} ,$$

and (5) becomes

$$\psi_{50} = \frac{1.7 \times 10^{-2} \rho p_a Q_a D_{50}}{18\eta D_j^3 p_o^2 \frac{\pi}{4} N} . \quad (6)$$

Assuming a constant jet velocity, Eq. (4) and Eq. (6) may be combined to obtain

$$D_{50} \sim p_o D_j$$

$$\text{and } Q_a \sim D_{50} D_j N .$$

These are fundamental relationships in low pressure impactor operation.  $D_{50}$  depends only on the internal pressure and nozzle size, whereas the external gas flow depends on the number of nozzles too. It is easier to obtain a small  $D_{50}$  value at low gas flow than at high gas flow. Small  $D_{50}$  at a high flow rate can be achieved only with a great number of nozzles.

The slip effect, which on the one hand enables the impaction of small particles, on the other hand reduces acceleration of the particles to the jet velocity. Particles not at jet velocity would have a smaller deposition

efficiency. An estimate of the slip in velocity is easily obtained from the basic equations of the impaction theory.<sup>6,8</sup>

The motion of particles in a nozzle of constant diameter can be described by equating the force of inertia of the particle to the force of viscous drag by the medium as shown in Eq. (7),

$$m\dot{v}_p = \frac{3\pi\eta D_p}{C} (v_p - v_j) , \quad (7)$$

where  $v_p$  is the component of velocity of particles in the direction of the jet,  $v_j$  is the jet velocity (parallel to the nozzle axis),  $m$  is the particle mass and is equal to  $\rho \frac{\pi}{6} D_p^3$ ,  $D_p$  is the particle diameter.

$$\text{On taking } \dot{v}_p = \frac{dv_p}{dx} \cdot \frac{dx}{dt} = \frac{dv_p}{dx} v_p .$$

Substituting and rearranging, one obtains

$$\frac{dv_p}{dx} = - \frac{18\eta}{\rho CD_p^2} \left( 1 - \frac{v_j}{v_p} \right) \quad (8)$$

and if  $v_j$  is assumed to be constant, then

$$\frac{v_p}{v_j} + \ln \left( 1 - \frac{v_p}{v_j} \right) = \left[ - \frac{18\eta}{\rho CD_p^2} \frac{x}{v_j} \right]_0^L . \quad (9)$$

At the limiting values of  $x$ , the following are true;

$$\text{at } x = 0, v_p \approx 0$$

$$\text{at } x = L, v_p \neq 0.$$

Applying Eq. (1) it follows that,

$$\frac{v_p}{v_j} + \ln \left( 1 - \frac{v_p}{v_j} \right) = - \frac{L}{\psi D_j} . \quad (10)$$

This equation is plotted in Fig. 3. Beyond  $L/(\psi D_j) = 10$  the slip in velocity is negligible. In practice, the region in which  $v_j$  is considered to be constant should be twice as large as the diameter.

The size distribution of the aerosol is obtained from the amounts of deposited material on the stages and the stage constants. T. T. Mercer<sup>12</sup> prefers the use of the effective cut-off diameter, ECD, rather than the mass median diameter, MMD, as the stage constants, because with the latter one depends much more on the aerosol size distribution than with the ECD. In the ECD approximation the efficiency curve is approximated by a step function. Below ECD the collection efficiency is presumed to be zero and above ECD the efficiency is unity. In this approximation the actual amount of material collected below ECD is compensated by the amount lost above ECD. The following shows how the size distribution of the aerosol can be evaluated in the ECD approximation if the relative amount of material on the impaction stages is known.  $N_i$  is the amount of material on stage  $i$ ,  $\eta_i(D)$  is the efficiency of deposition of particles of diameter  $D$ .  $n(D) \times dD$  is the number of particles in the size range  $D \dots D + dD$ .

$$N_1 = \int_{D=0}^{D=\infty} n(D) \eta_1(D) dD = \int_{ECD_1}^{\infty} n(D) dD \quad (11)$$

$$N_2 = \int_0^{\infty} n(D) \eta_2(D) [ (1 - \eta_1(D)) ] dD = \\ \int_0^{\infty} n(D) \eta_2(D) dD - \int_0^{\infty} n(D) \eta_1(D) \eta_2(D) dD =$$

$$\int_{ECD_2}^{\infty} n(D) dD - \int_{ECD_1}^{\infty} n(D) dD = \int_{ECD_2}^{ECD_1} n(D) dD . \quad (11a)$$

$$N_i = \int_{ECD_i}^{ECD_{i-1}} n(D) dD . \quad (11b)$$

Assuming infinitesimal steps, the size distribution is obtained:

$$n(D) = \frac{N_i}{ECD_{i-1} - ECD_i} . \quad (12)$$

It is easy to see from Eq. (11) that ECD depends on the aerosol size distribution. Therefore in practice the  $ECD_i$  are usually not known and the smoothness (and hence the accuracy) of the frequency distribution [ $n(D)$ ] is limited by the number of impactor stages. In a reasonable approximation, ECD is replaced by the stage constants ( $D_{50}$ ) which is only a characteristic constant of the impaction stage and does not depend on the aerosol size distribution. The closer the efficiency curve approaches a step function the more accurate this approximation becomes.

### 3. EXPERIMENTAL APPROACH

#### 3.1 General Assembly

The general assembly used in most cases is shown schematically in Fig. 4, and a photograph of the assembly is given in Fig. 5. Air is drawn by suction through the furnace (in which particles are formed by vaporization and condensation in the cool air stream) and through valve V-2. A dryer unit D and a charcoal cartridge F reduces humidity and the concentration of natural aerosol. The air flow is

controlled by valve V-1 and indicated by the flow meter R-4. After steady state conditions for the furnace temperature are established, the by-pass to the 70-liter containment tank (V-2) is closed and the containment tank is filled with the particles by suction through valve V-5. Filter samples taken upstream of V-2 enable one to check the approach of a steady-state particle generation rate.

The particles are enclosed in the containment tank for a certain time (about 1 hr). During this aging period, the mass median diameter increases by agglomeration until the right size for the sampler is reached. Before the particles are directed into the sampler, steady flow conditions in the sampler are established by suction of the pump below the sampler and flow through an open by-pass line, V-5. The particles are directed to the sampler, by closing valve V-5 and opening V-4. At the same time the flow from the furnace to the containment tank is replaced by a supply of cleaned air.

The low pressure in the sampler is generated by a pressure drop at a flow nozzle and by the amount of air added through valve V-7. If desired, the air flow through the sampler can be changed by another nozzle size. The first stage of the sampler is positioned in a distance far enough from the nozzle (about 5 times the sampler diameter) so that it can be assumed that the spread of the jet is sufficient to cover the whole diameter of the first stage. All particulate matter penetrating the stages are held up in a back-up filter. Provisions are made to measure the pressure at several points in the sampler as indicated. Additional flow controls are provided by flow meters R-1, R-2, and R-3. A closer look at the arrangement of the flow nozzle, impactor stages and back-up filter is presented by Fig. 6.

The first operation in nuclear safety research was performed during a CRI run, in which the behavior of released fission products was the main interest. Two gas samples were taken and analyzed with the Low-Pressure Cascade Impactor. A description of the Containment Research Installation (CRI) and the release of simulated fission products is reported elsewhere.<sup>13</sup> More experimental details will be given in Section 3.6.

### 3.2 Particle Generation

In the cases in which only the function of the low-pressure cascade impactor was tested and a variable supply of aerosol was acceptable, material was vaporized from an open boat and condensed in a cool air stream. The boat was inserted into a tube heated by an electric furnace (see Fig. 4). By this technique, particles from nichrome wire, PbI<sub>2</sub> and CsNO<sub>3</sub> were generated.

To achieve a more reproducible size distribution and number concentration, the material was vaporized into a gas stream of low linear velocity over the hot surface, so that the solid-vapor equilibrium was only slightly disturbed. Under these circumstances the vaporization rate is much less (than in the case in which the partial pressure is much lower than the equilibrium value). The vaporization is also more independent of surface aging. The gas volumes drawn from the saturated atmosphere always contain the same amount of material per unit volume, but a high flow rate requires a high effective surface. A quartz tube, 18 mm I.D. by 200 mm long was filled with fine quartz wool on which the aerosol material (NaCl) was adsorbed. 1.4 g of fine quartz wool was wetted with 2 g NaCl in 40 cc H<sub>2</sub>O and dried slowly. Care was taken to limit the amount of salt solution so that it did not drip from the quartz wool prior to drying.

Filter samples taken downstream indicated some wall loss at lower flow rates. The NaCl concentration in air continuously increases as air flow increases (Fig. 7). This shows that the saturated partial pressure at the evaporating surfaces was not disturbed, otherwise the curve would bend down.

The aerosol taken in the CRI experiment was produced as described by G. W. Parker et al.<sup>13</sup>

Some experiments were performed at the University of Minnesota with spherical particles of known size and a very narrow size distribution, in order to calibrate the low-pressure cascade impactor. These particles were produced either in a atomizer-impactor combination from a uranine dye solution or in a spinning disk generator from a uranine dye solution with methylene blue added, as described by K. T. Whitby et al.<sup>14</sup> The characteristic data with these particles are summarized in Table 1.

### 3.3 Low-Pressure Cascade Impactor Mark I

The first tests were performed with the Andersen Sampler 0101,<sup>15</sup> the deposition efficiency of which has been measured, for instance, by J. C. Couchman.<sup>17</sup> The stage constants were calculated as a function of pressure using Eq. (6) and assuming that the reported impaction parameter,  $\psi_{50} = 0.2$ , is unchanged under low pressure operation. The results are shown in Fig. 8 in which the stage constants are plotted versus the stage number for different pressures and specific gravity of particles. Decreasing pressure and increasing specific gravity will lower the stage constants in all stages. At about 40 mm Hg the sampler covers just the size range of interest. On this basis the work was started with the Andersen Sampler 0101 after some modifications were done (the modified Andersen Sampler is called Mark-I).

Table 1. Characteristic Data of the Uranine Aerosols

Generator	Material	MMD ( $\mu$ )	$\sigma_g$
Spinning disk	Methylene blue plus uranine	3.5	1.15
Spinning disk	Methylene blue plus uranine	1.5	1.15
Atomizer-impactor	Uranine	0.26	1.67
Atomizer-impactor	Uranine	0.10	1.41
Atomizer-impactor	Uranine	0.049	1.49
Atomizer-impactor	Uranine	0.028	1.45

The MMD's of the particles generated in the spinning disk device were obtained by counting the particles which were deposited on filter media under the light microscope. The other MMDs are known from previous calibrations.<sup>14</sup>

The density of the particles was 1.3 g/cm<sup>3</sup>.

Petri dishes filled with a liquid were used in the original design as sample area. They were replaced in the modified design by sample plates made out of aluminum in order to have a more accurate adjustment of the clearance between sample plate and hole plate, as well as to provide a simple throw-away sample plate. This modified sampler is shown in Fig. 9. The sample plate is fixed with some vacuum grease on a support plate. (In Fig. 9, the sample plate is black and the white spots are deposited NaCl particles.) Each support plate is connected by three screws to the stage. The clearance between sample plates and hole plates was chosen for all stages to be three times the hole diameter. Thus, the performance of the stages are easily comparable. Smaller clearance would tend to make the efficiency curve approach a step function,<sup>7,16</sup> but would cause an intolerably high radial pressure drop. Some of the interesting data of the Mark-I are listed in Table 2. The hole diameters were measured by an optical apparatus.

Tubes were connected to each stage to allow pressure measurements. This is important because the pressure at each stage has to be known in order to calculate the stage constant according to Eq. (6). Pressure and pressure drop at the sampler is shown in Fig. 10 as a function of the inlet air flow (flow adjusted upstream of the sampler).

As described in the Appendix, the stage constants\* of the Andersen Sampler under low pressure were obtained by an experimental method. Calculated and measured stage constants\* do not agree in the first stages but become quite comparable for stages 4 to 6. Some reasons for this behavior are discussed in the Appendix. Based upon the calibration, the stage constants for each stage were calculated for several specific gravities of particles using Eq. (6). The pressure at each stage was taken at an air flow rate of 8 liters/min. Figure 11 graphically shows the results.

---

\*Particle diameter cutoff point or  $D_{50}$  in Eq. (6).

Table 2. Hole Diameters and Clearance Between Plates  
for the Mark-I Impactor

Stage No.	$D_J$ (cm)	$L^*$ (cm)	$N^{**}$
1	$1.1 \times 10^{-1}$	$4.2 \times 10^{-1}$	400
2	$8.97 \times 10^{-2}$	$3.1 \times 10^{-1}$	400
3	$7.37 \times 10^{-2}$	$2.8 \times 10^{-1}$	400
4	$5.22 \times 10^{-2}$	$2.0 \times 10^{-1}$	400
5	$3.43 \times 10^{-2}$	$1.25 \times 10^{-1}$	400
6	$2.44 \times 10^{-2}$	$9.0 \times 10^{-2}$	400

\*  $L$  denotes clearance between sample plate and hole plate.

\*\* Denotes number of holes.

In order to prove the uniformity of deposition, the black painted impaction plates were heavily loaded with white NaCl particles. The size distribution was not wide enough to cover all 6 stages, therefore only the last 4 stages show particle deposition in Fig. 12. The sizes of the spots are not as equal as they should be, indicating slight differences in deposition efficiency between the jets.

### 3.4 Low-Pressure Cascade Impactor Mark-II

Besides the modified Andersen Sampler (Mark-I), our own design (Mark-II) was built. This model was specially designed for low pressure operation, small pressure drop, easy de-contamination and quick exchange of sample plates. Again, as for the Andersen Sampler, the sample plates were designed for easy fabrication so that they could be discarded after one use and reduce the efforts required for decontamination. Hole diameter and number of holes were calculated to provide a desirable increase in  $D_{50}$  of a factor of three from stage to stage for particles of specific density 6 g/cc. The impaction parameter was assumed to be 0.15 in this calculation. Smaller clearances between sample plates and hole plates were used than in the modified Andersen Sampler to improve the particle size separation, i.e., to make sharper separations. Design data are shown in Table 3. Details of the design may be taken from Figs. 13 and 14.

Sealing between the stages is provided by O-rings. Spring loaded pins press the sample plates against three points of the support. This allows the sampler to be operated in any orientation. Tubes are connected to the stages to allow pressure measurements. At the standard air flow of 8 liters/min, the pressure drops listed in Table 4 were observed.

Table 3. Design Data for Sampler Mark-II

Stage No.	$D_J$ (cm)	$L^{**}$ (cm)	N	x* (cm)	y* (cm)	d* (cm)
1	0.56	0.20	20	0.50	3.3	1.0
2.	0.386	0.14	20	0.44	3.3	1.0
3	0.257	0.14	20	0.44	3.3	1.0
4	0.15	0.10	38	0.40	2.8	0.5
5	0.10	0.05	51	0.35	2.7	0.4
6	0.071	0.05	49	0.35	2.7	0.4

\*Symbols refer to dimensions shown in Fig. 13.

\*\*Denotes clearance between sample plate and hole plate.

Table 4. Pressure Drops (mm Hg)

$\Delta P_{1-6}^*$	$\Delta P_4$	$\Delta P_5$	$\Delta P_6$	$P_6^{**}$
19.5	0.9	3.1	14	22.7

\* $\Delta P_i$ , pressure drop at stage i.

\*\* $P_6$ , pressure at sample plate 6.

A photograph of the stages is shown in Fig. 15. The white spots represent deposition of NaCl particles.

It was found in the test, described in the Appendix, that the calculated stage constants\* and the experimental ones are practically identical for all stages, showing that the chosen impaction parameter ( $\psi_{50} = 0.15$ ) was just the right one. With this verified value, stage constants for a greater variety of specific gravity of particles were calculated. The results of the calculations are plotted versus the stage number in Fig. 16. As in Fig. 11, these stage constants are to be expected only at an air flow rate of 8 liters/min and at the corresponding pressures at each stage.

The uniformity of the deposition was checked (as it was for Mark-I) with a heavy load of solid NaCl particles on the black painted impaction plates. Depositions of particles were found on all 6 stages (see Fig. 17), and the particle spots on each stage are nearly equal in intensity. The particle size distribution was the same in both experiments, thus Figs. 12 and 17 are comparable. It is apparent that deposition was more uniform and that more stages cover the same particle size range in Mark-II (Fig. 17) than in Mark-I (Fig. 12).

### 3.5 Method of Analysis

The size distributions of the aerosols under investigation were evaluated by the material distribution among the impaction plates, the back-up filter and the stage constants.

In case of uranine particles, these particles were removed from the sample plates by dissolving in a known quantity of water. The intensity of fluorescence of the wash water was measured. It was proved that even from silicon coated surfaces, which were usually used, nearly all uranine

---

\*Particle diameter cutoff point or  $D_{50}$  in Eq. (6).

particles were dissolved and only a negligible amount remained. By the calibrated reading on a fluorometer, the total mass of deposition could be calculated.

The other aerosols were radioactive tracered, in order to calculate their relative mass distribution among the stages from the radioactivity sampled on each impaction plate. A homogeneous mixture between tracer and bulk material was achieved by neutron activation in the case of nichrome wire (Cr-51) and CsNO<sub>3</sub> (Cs-134). Radioactive PbI<sub>2</sub> was produced by mixing inactive iodine solution with I-131 tracer solution before the PbI<sub>2</sub> was precipitated. Neutron activated NaCl (Na-24) was dissolved in water and then precipitated on the quartz wool. A homogeneous distribution of Na-24 in the total amount is therefore also established. The relative radioactivity of the deposited material was measured by  $\gamma$  counting.

The mass of the NaCl aerosol per volume of air was checked downstream of the NaCl furnace by weighing and  $\gamma$  counting a Gelman GA-4 filter sample. This also provided data of the mass deposition on the sample plates by comparing the  $\gamma$ -count of the sample plates and the filter and from the known mass deposition on the filter.

### 3.6 Containment Research Installation (CRI) Experiment

The release of fission products from molten UO<sub>2</sub> and their behavior under reactor accident conditions was studied in run 107 in the Containment Research Installation (CRI). In order to lower the impractically high activity of a high burnup fuel element, unirradiated UO<sub>2</sub> was heated and the released fission products were simulated by radioactive tracered fission product elements according to a technique described by G. W. Parker et al.<sup>13</sup> Separately vaporized iodine, cesium, ruthenium, and tellurium passed the hot UO<sub>2</sub> zone in a steam atmosphere. Most of the condensation

processes and particle coagulation took place in the UO<sub>2</sub> furnace tube and the transfer line to the reactor core. Then, entering the containment tank of the CRI the particle coagulation rate became very small because of the high dilution of their number concentration. Data of the amount of vaporized materials and their distribution on the components of the CRI were not available at the time this report was written. They will be published in the Annual Progress Report of the Nuclear Safety Program 1967.

In its first Containment Research Installation test, two impactor gas samples were taken. The first gas sample of 27 liters STP was taken from the containment atmosphere between 15 and 18.5 min after meltdown and mixed with dry air in a 70-liter vessel. A second sample of 36 liters STP was transferred between 63.5 and 68 min after meltdown to the 70-liter vessel and also mixed with dry air. The vessel was swept with fresh air before the second sampling. The gas flow rate from the CRI into the vessel was limited by an orifice or nozzle. Steam condensation in the pipe between the CRI and the sampling vessel and the flow nozzle device was eliminated by heating the walls to about 120°C.

Since the primary purpose of the cascade impactor is size classification of radioactive fission product particulates, the presence of a large amount of gaseous radioiodine could confuse the results by non-selective plateout on the sample plates. In order to minimize this effect, silver screens were used in conjunction with the impactor to reduce the fraction of gaseous iodine. The efficiency of silver screens (80 by 80 mesh silver plated copper screen) for adsorbing gaseous iodine and the corresponding low retention for sub-micron particles was tested. In the iodine test, the iodine was produced by the bichromate method and the iodine deposition checked by the radioactivity of its tracer I-131. The penetration of NaCl particles was also measured with the screens in place.

The Low-Pressure Cascade Impactors were fitted with three silver screens in front of 5 impaction plates followed by two additional silver screens and the back-up filter. Both samplers were used in this experiment, the first gas sample was analyzed by the Mark-I and the second by the Mark-II. Fifty-eight liters (STP) of the gas contents of the vessel were passed through the sampler. All impaction plates were silicone oil coating as described in Chapter 4.2.

#### 4. RESULTS AND DISCUSSION

##### 4.1 Experimental Verification of the High Retention of Small Particles in the Cascade Impactor Under Reduced Pressure

In order to test the retention efficiency of the modified Andersen Sampler for small particles under low pressure, two runs were performed, one at 40 mm Hg and the other at 750 mm Hg. A 3-hr agglomeration time in the 70-liter containment tank was assumed to be sufficient to equalize slight differences in the initial particle size distribution and concentration for both aerosols under test. Of course, the sample conditions were nearly the same in both cases.  $\text{CsNO}_3$  with Cs-134 tracer was heated from an open boat, see 3.2. The fractional deposition of Cs-134 activity on the stages and filter is given in Fig. 18. It is evident that the sampler was efficient enough under low pressure but not under normal pressure. The same test was performed with  $\text{PbI}_2$  indicating the high efficiency for small particles too. In all other cases, the main portion of the activity was found in the sampler and only a small portion on the back-up filter. This means that the low-pressure cascade impactor was adequately efficient for the aerosol under investigation. The operation of two Andersen Samplers in series is also instructive, one operating in the designed way (that means normal pressure), and the other one under reduced pressure.

Results of such an experiment are given in Table 5. The air in this experiment (No. 57) first passed the Andersen Sampler then the flow nozzle which produces the pressure drop and finally entered the modified Andersen Sampler (Mark-I). Experiment No. 50 in which the first Andersen Sampler was left out is given for comparison. Both experiments were performed at 8 liters/min flow rate, the Andersen Sampler at atmospheric pressure and the Mark-I at about 40 mm Hg. NaCl particles were used as the aerosol. The deposition is expressed in  $\mu\text{g}$ . On comparing both experiments, one sees no significant difference in the deposition. Size distribution and number concentration are practically not affected by the Andersen Sampler placed before the Mark-I.

The material found on stages 1, 2, and 3 of the Andersen Sampler is about constant and probably due to collection by interception and diffusion. The amount of material deposited by impaction increases from stage 4 to 6 without going through a maximum deposition, as found on the Mark-I. It seems, that the stage constant of stage 6 of the Andersen Sampler lays between the one of stage 2 and 3 of the Mark-I, indicating a shift of stage constants at low pressure operation over at least three stages.

#### 4.2 Particle Loss

Particles are not only deposited on the impaction plates, they are found also on the walls of the sampler. Several wall loss studies have been reported<sup>8,16,18</sup> and loss mechanisms have been discussed, but the results depend so much on the impactor design and operating conditions that they cannot be generalized. It was decided to study the wall loss with a particle size close to the stage constants of stage number 3 or 4 and a narrow size distribution which should be more instructive, in studying the bounce of particles from the impaction plates, than the use of a wider size

Table 5. NaCl Deposition in  $\mu\text{g}$ 

Experiment No. 50	Experiment No. 57
Andersen Sampler	
Stage 1	9.8
Stage 2	9.7
Stage 3	9.9
Stage 4	10.2
Stage 5	28.2
Stage 6	248.5
Sub-total	316.3
 <u>Mark-I</u>	
Stage 1	2.5
Stage 2	5.8
Stage 3	213.5
Stage 4	4620.0
Stage 5	1178.0
Stage 6	102.0
Filter	28.7
Total	6150.5
 <u>Mark-I</u>	
Stage 1	4.2
Stage 2	6.9
Stage 3	665.0
Stage 4	4600.0
Stage 5	773.0
Stage 6	38.7
Filter	23.3
Sub-total	6111.1
GRAND-TOTAL	6427.4

distribution. Furthermore, maximum deposition on the middle stages seems to be more realistic with respect to application in the CRI experiment, see 4.3.

NaCl particles were selected for these experiments, because they are easily washed off the components with water and then recovered in a cation exchanger (DOWEX 50 W x 12). Another advantage is that the NaCl aerosol generator gives a reproducible production rate, which is necessary for comparing depositions under different conditions. About 10 mg of NaCl particles were enclosed in the 70-liter containment tank for 1 hr. During this time the MMD grew to the desired size. Then part of the volume was filtered in either the Mark-I or Mark-II.

4.2.1 Particle Loss on the Wall. Wall loss studies were performed on both types of cascade impactors, Mark-I and Mark-II. The flow rate through the sampler was adjusted by the size of the flow nozzle to 8 liters/min in experiments Nos. 48, 50, and 56 and to 0.8 liters/min in No. 61. The sampling time was chosen according to the desired amount of deposition. Table 6 shows the amount of material found on the nozzle, nozzle stage (tube between nozzle and impaction stage 1), walls of impaction stages 1 to 6 and filter stage, in percent of the total amount on impaction plates and back-up filter. In general, as the total amount of material increases the relative loss increases. But the relative loss as a function of stage number seems to be due to two processes, one whose importance is decreasing with increasing stage number superimposed on a second process, which leads to a loss proportional to the amount of deposited material in the corresponding stage. Comparing the experiments Nos. 48, 56, and 61, the first process (considered as background) depends on the flow rate, whereas the second one depends on the amount of deposition. The loss due to the

Table 6. Particle Loss on Walls

Experiment	No. 48 Mark-II	No. 50 Mark-I	No. 56 Mark-II	No. 61 Mark-II
Total amount on plates and back-up filter ( $\mu\text{g}$ )	5529	6151	849	380
Loss related to total amount (%)				
Nozzle	0.31			1.74
Nozzle-Stage	0.21			
Wall of Stage 1	0.070	0.12	0.091	-
Wall of Stage 2	0.094	0.16	0.054	0.55
Wall of Stage 3	0.154	0.39	0.067	0.17
Wall of Stage 4	4.25	0.78	0.375	0.24
Wall of Stage 5	2.04	0.28	0.137	0.12
Wall of Stage 6	0.04	0.037	0.039	0.06
Filter Stage	0.010	0.0067	0.006	-
Flow rate (liters/min)	8	8	8	0.8

second process seems to increase relatively faster than the deposition load.

The background effect (first process) is probably related to loss by diffusion, because it increases at lower flow rates. Particle bounce from the stages causes the second effect. This effect is less in the Mark-I in which the jet number is higher, but it may be noticed that the background loss is higher in the Mark-I.

Material loss at the nozzle, within the tube between nozzle and first stage and in the filter stage, is small. The loss on the smaller nozzle in Experiment No. 61 is higher but could be reduced by redesigning the intake nozzle.

4.2.2 Particle Loss from the Impaction Plate. Particles with high inertia which should settle by impaction on a surface will bounce if the collision is elastic and the kinetic energy higher than the energy absorbed by the surface. In cases in which the particles are deformed or break into fragments, the collision is to be considered inelastic and part of the energy is absorbed by these processes, but this will not necessarily reduce bouncing. Inelastic collisions can also be obtained by coating the surface with a liquid, as reported by several authors. This would reduce bouncing, because kinetic energy is absorbed in the liquid and the adhesion force is increased too.

Some of the particles which bounce off the impaction plate will even penetrate the next stage, because the deposition efficiency is not 100% for this size and bounce becomes easier at the higher velocity on the next stage. Thus, some of the particles penetrate all stages intact, and finally get caught on the filter. If the material transport from one stage to the other by bouncing is neglected, then the size distributions based upon the material distribution among the stages will be incorrect.

The influence of coating, load and particle velocity on the material distribution among the stages was investigated in both samplers. The particle size distributions and number concentrations were kept as constant as possible in all experiments. The plates were coated with 1 cc of a 7% solution of Dow Corning Silicone Oil 250,000 cs in hexane. On evaporation of the hexane, each impaction surface was left with an oil coating of several microns in thickness.

From the amount of material found on each stage, the cumulative material distribution was calculated and plotted versus the stage constants in Fig. 19 for Mark-II. In general, the results for Mark-I are the same and are not given. Material found on stage 1 was not taken into account because it was considered as contamination; probably due to interception and diffusion losses. The particle size distribution of the NaCl aerosol is expected to be log-normal, that means, this size distribution is represented by a straight line in the type of diagram used in Fig. 19. But all curves reported deviate from a straight line at small particle diameters. The higher the load of NaCl particles, the more the curves bend down at small particle diameters. In addition to the load effect, the coating of the impaction surface appears to be very important too, but reducing the particle velocity (by a factor of 5 in Experiment No. 61) had no significant effect. The effect of less load (than indicated upon the size distribution curves) could not be investigated because of difficulties in detecting small amounts of radioactivity. On the other hand, the specific activity was as high as safe loading and handling of the NaCl furnace would allow.

A one percent material loss from stage No. 4 would explain the deviation of the curves from the straight line for Nos. 64 and 65. If particles are lost from one stage and deposited on the next ones, a higher apparent amount of small particles is indicated than that which is in accordance with a log-normal particle size distribution.

Particle bounce from the stages seems to occur by two mechanisms, one which is influenced by coating and the other one which depends on the load. The first mechanism associated with impaction and adhesion onto the impaction surfaces and the second one is associated with the same processes onto particles already deposited. Particle bounce from the surface is reduced by the silicone film but, on the other hand, interaction with material already deposited is not much affected by the coating. The wall loss, studied in the previous chapter, is not as easy to explain on the basis of simple particle bounce. Because of the large open space between the impaction plate and the wall, the gas velocity is very low and the efficiency for elastically bounced particles to impact onto the wall is very low. But if fragments of particles are released from the impaction plates, as a consequence of impact, their deposition efficiency onto the walls is higher as a result of their greater slip and higher diffusion rates. Fragmentation of particles is more easily obtained during impact on a bed of settled particles than on the inelastic coating. This means that one has to deal with both intact particles and particle fragments in the bounced material.

#### 4.3 Radioiodine and Radiocesium in the CRI, Analyzed by the Low-Pressure Cascade Impactor

Gaseous radioiodine may plate-out on impaction plates and therefore interfere with the radioactive analysis of particulates. But it was demonstrated that silver screens at the front end of the sampler are very effective in reducing the amount of gaseous iodine (molecular iodine) without significantly retaining the particulates. These tests were performed with molecular iodine produced by the bichromate method and NaCl particles. Both runs were accomplished with the Mark-II fitted with three silver screens in front of stage 1 and coated plates. The results are shown

in Table 7. Less than 1% of the molecular iodine was found on all 6 stages. The load of iodine on the screens was unnecessarily high, so that with less iodine loading, the penetration through the screens should be even less. 1.5% of the particles were lost on the screens which is acceptable.

It was also decided to place two silver screens in front of the back-up filter in the CRI experiment in order to lower the load of gaseous iodine on the filter. The transfer of the gas sample from the containment tank of the CRI into the 70-liter vessel was quickly accomplished, the Low-Pressure Cascade Impactor was hooked up and a known part of the atmosphere passed over the sampler. The amount of radioactive material plated out in the vessel and the distribution of the Cs-134 and I-131 nuclides among screens, plates and back-up filter was then evaluated by  $\gamma$ -counting and pulse height analyses. Table 8 shows the result of both gas samples. The listing sequence of tank retention, of silver screens, impaction plates, second silver screens and back-up filter corresponds to the actual arrangement. In cases in which a proper I-131 activity evaluation was impossible because of high Cs-134 background, the upper possible limit of this nuclide was estimated from the shape of the printed  $\gamma$ -spectrum. In none of the  $\gamma$ -spectra of the impaction plates was there found an indication of I-131. This should be the case, if the iodine activity is higher than 1% of the cesium activity in Sample 1 and higher than about 2% in Sample 2. Because of some uncertainty in the iodine plate-out in the second sample, the relative iodine distribution is given only for Sample 1. Also because of high Cs-134 background the Te-125m and Ru-101 nuclides could not be detected with the 3" x 3" NaI crystal.

One important result of this experiment is the fact, that the amount of particulate iodine in the first sample is obviously very low, because the iodine activity on the

Table 7. Relative Distribution of Gaseous Iodine and  
NaCl Particles on Screens, Stages and Filter

	Relative Amount in %	
	Gaseous Iodine	NaCl Particles
Screen 1 . . . 3	98.02	1.50
Stage 1 . . . 6	0.72	98.06
Filter	1.26	0.44

Table 8. Distribution of Radioiodine and Radiocesium Between  
the Sampling Tank and the Low-Pressure Cascade Impactors

	1st Sample Analyzed by Mark-I		2nd Sample Analyzed by Mark-II	
	I (%)	Cs (%)	Cs (%)	
Total Inventory	100	100	100	
Plate Out Inventory (Sampling Tank)	97.6	55.6	52.4	
Silver Screen 1	.55	.15	.23	
Silver Screen 2	.16	.11	.13	
Silver Screen 3	.08	.12	.14	
Total	0.70	0.38	0.50	
Impaction Plate 2	<.02	.55	5.1	
Impaction Plate 3	<.12	7.4	29.5	
Impaction Plate 4	<.82	33.6	12.2	
Impaction Plate 5	<.1	2.5	.22	
Impaction Plate 6	<.0009	0.002	.009	
Total Particulates	<1.0*	44.0*	47.029	
Silver Screen 4	.11	-	-	
Silver Screen 5	.134	-	-	
Filter	.008	.02	.0007	

\* Since an approximately equal amount of Cs-134 particulate activity plated out in the sampling vessel as was collected on the impactor plates; it is inferred that not more than a similar ratio existed between the radioiodine in gaseous form and that in a particulate form in the sampling vessel.

impaction plates was estimated to be less than 1% of both the Cs-134 activity and the total iodine whereas the ratio between iodine and cesium was about one in the CRI atmosphere at the time of the first sampling. This means that most of the iodine in the gas phase was still in the reactive gaseous state. May pack samples of the containment tank atmosphere indicate that the iodine activity in the second sample was only 1/4 of the first and the cesium activity dropped by about 20%. But one cannot determine on this basis whether or not the relative amount of the particulate iodine was higher in the second sample than in the first.

The amount of particles lost on the screens is only about 1% which is in agreement with the data found for NaCl particles. Allowing for the fast plate-out of molecular iodine in the connecting pipe and the 70-liter vessel, the relatively low I-131 activity on the screens becomes credible. In comparing the Cs-134 deposition on the two samplers, the different stage constants for the same stage number has to be recognized. Both samplers were very effective in holding back particulates. The cesium activity on the back-up filters is supposed to be contamination by bounced particles. Stage 1 was not used in either sampler, because the stage constants were too high over the mass median diameter of the particles.

The cumulative deposition of particles carrying Cs-134 was calculated from the relative distribution of Cs activity on the impaction plates and plotted against the stage constants in Fig. 20. The recording of the material transfer into the containment tank of the CRI (by  $\gamma$ -detection) showed that the cesium transfer was accomplished before the main part of  $\text{UO}_2$  particles was released. Thus, the specific gravity of cesium oxide (4 g/cc) was applied to obtain the stage constants from Figs. 11 and 16. Further reaction between cesium oxide particles and  $\text{UO}_2$  particles in the

containment tank would be coagulation which occurs at a negligible rate. The mass median diameters (MMD) found were  $0.33 \mu$  for the first sample and  $0.52 \mu$  for the second one. It is assumed that the particles entered the containment tank with these relative high MMD values, because the mass concentration in the tank was only about  $0.001 \mu\text{g}/\text{cc}$ , which is too small to produce such a high MMD by coagulation in a short time. On the other hand, the particle concentration was high in the transfer line and the transfer time (in the range of seconds) was long enough, so that most of the coagulation took place there. The particle sizes were essentially frozen by dilution of the number concentration into the containment tank. This explains the small increase in MMD during a time of about 50 min between the two samples.

## 5. SUMMARY

Submicron particles are an important subject of investigation in nuclear safety research. Instruments which would separate these particles into different size fractions, and make each size fraction available for further analysis are of great interest. Cascade impactors are ordinarily limited to particle sizes greater than  $0.5 \mu$  and are therefore not adequate for this task. But this range can be extended to very small sizes by operating the impactor at low pressure. This makes the cascade impactor of genuine use in nuclear safety research. Small particles which would not impact under normal pressure are deposited on the impaction plates, at reduced pressure, by a slip effect in the gas stream. The range of application is thus extended to particles of less than  $0.01 \mu$  diameter. Two samplers were calibrated and tested with several aerosols. One was a modified Andersen Sampler (Mark-I). A second sampler (Mark-II) was designed and built to better meet our requirements. Both samplers were

first demonstrated in nuclear safety research during CRI Run No. 107. Simulated fission products were analyzed and it was estimated that the particulate iodine contributed not more than one percent to the total iodine content.

The Mark-II sampler is recommended for use in Nuclear Safety containment research. It separates particles in the size range about  $0.01 \mu$  to several microns. It is easily assembled or disassembled — for instance, in a hot cell. (Disassembly and reassembly for another sample can be accomplished on cold material in a few minutes.) It is designed with throw-away plates which facilitate decontamination and measurement by radioactivity.

Design data are given in the report. Calibration data are given in Fig. 11 (for Mark-I) and Fig. 16 (for Mark-II) for flow rates of 8 l/min. Calibration for other flow rates can be calculated [by means of Eq. (6)].

Bounce of particles from impaction plates can be reduced by properly coating the impaction surface and by avoiding an overload of particles. In general, a barely visible deposit of solid particles represents the best load.

## 6. ACKNOWLEDGMENT

We wish to acknowledge the Particle Technology Laboratory at the University of Minnesota for the use of their aerosol generators. In particular, the aid and hospitality of B.Y.H. Liu and A. R. McFarland are acknowledged.

We wish also to express appreciation for the help of G. E. Creek for supplying a computer code for some of the calculations.

## 7. APPENDIX: CALIBRATION OF THE LOW-PRESSURE CASCADE IMPACTORS

Both Low-Pressure Cascade Impactors were calibrated with aerosols of a very narrow size distribution. The calibration data were presented in 3.2, Table 1. The technique of particle generation has been reported<sup>14</sup> and shall not be discussed here.

Each time before sampling with the cascade impactor was started, the generators were operated for a certain time to establish steady state conditions in particle size and number concentration. The sampling time was kept as short as possible to avoid overloading the impaction plates with particles. Normally the particle spots on the plate with the highest particle density were just visible. All impaction plates of the presented experiments were coated with several microns of Dow Corning Silicone Oil 250,000 cs.

The aerosol particles were detectable by the fluorescence of uranine. Therefore the deposited material on impaction plates and back-up filter was washed off with water, and the amount of uranine evaluated in a fluoremeter. Although the plates were coated, washing with water was very effective in dissolving practically all the uranine. The amount of uranine particles per volume of wash water is presented in Table 9. The Mark-I impaction plates were washed in 20 cc H<sub>2</sub>O, the Mark-II plates in 40 cc H<sub>2</sub>O. Open spaces in the table indicate that the corresponding stages were not used.

In all runs with the exception of Nos. 17 and 18, the inlet air flow rate was 8 liters/min. This rate was reduced to 1/10 of that value in Nos. 17 and 18. The pressure inside the cascade impactor was maintained constant by adding extra air (see Fig. 4, valve V 7). The maximum deposition was shifted under reduced flow in the Mark-I by

Table 9. Uranine Concentration,  $\mu\text{g}/\text{cc}$ 

Mark-I plates washed in 20 cc  $\text{H}_2\text{O}$   
 Mark-II plates washed in 40 cc  $\text{H}_2\text{O}$

Mark-I						
Run	14	16	18	22	20	12
MMD ( $\mu$ )	3.5	1.5	1.5	0.26	0.1	0.049
Stage 1	0.0026					
Stage 2	0.138	<0.001				
Stage 3	0.64	0.43	0.0014	0.0102	0.017	0.0012
Stage 4	0.005	0.090	0.0046	0.0485	0.0046	0.0295
Stage 5		0.0013	0.42	1.20	0.61	0.295
Stage 6				0.113	0.595	0.137
Filter	0.003	<0.003	0.0084	0.060	0.006	0.0066
Total	0.7886	0.5213	0.4344	1.4317	1.2321	0.4693

Mark-II						
Run	13	15	17	21	19	11
MMD ( $\mu$ )	3.5	1.5	1.5	0.26	0.1	1.049
Stage 1	0.054	0.0016	0.0012			
Stage 2	0.315	0.064	0.0028	0.0043		
Stage 3	<0.001	0.15	0.054	0.0011	<0.001	0.0010
Stage 4		0.0013	0.130	0.14	0.00275	0.0022
Stage 5		<0.001	0.0145	0.45	0.24	0.047
Stage 6				0.080	0.074	0.175
Filter	<0.003	0.0024	0.0017	0.0073	0.0054	0.0076
Total	0.369	0.2193	0.2042	0.6827	0.3221	0.2328

2 stages, but in the Mark-II only by one stage. From a theoretical consideration, a shift by two stages is expected. Therefore, it is possible, that as a result of confusion of the data for Run No. 17, the data are plotted on one stage number too low. In the final graph, Fig. 22, they are plotted where they are presumably supposed to be.

In order to evaluate the stage constants, first, the particle size distributions were drawn as 6 straight lines in a log-probability diagram. MMD's and  $\sigma_g$ 's are known (Table 1). Then the percent of the total uranine particles which penetrated each stage was calculated. Table 10 shows the results. Inserting the percentage of each stage (Table 10) in the right straight line, particle sizes are obtained which are identical to the stage constants of the corresponding stage.

The quality of this procedure is better the wider the size distribution of the aerosol is with respect to the size range in which the impaction efficiency is increasing from zero to one-hundred percent. For instance, a step function would result in a very accurate evaluation of the particle size at the step. On the other hand, a realistic efficiency curve and an ideal monodisperse aerosol would not be handled with this method. In practice the points close to the 50% point are of higher accuracy.

Only about half of all available data in Table 10 were finally used, these values are indicated by a star. The selection of just these values was not mystical. Numbers above 99% are not very reliable because of contamination by diffusion or interception loss. At the stages with numbers less than 1%, contamination by bounced particles is possible and the values may be too high. The procedure of obtaining the stage constants works best with numbers close to 50%.

Table 10. Percentage of Total Uranine Particles  
Which Penetrate Each Plate

Mark-I						
Run	14	16	18	22	20	12
MMD ( $\mu$ )	3.5	1.5	1.5	0.26	0.10	0.049
Stage 1	99.67					
Stage 2	81.2*					
Stage 3	0.64	17.5*		99.3		99.75
Stage 4		0.25	98.94*	95.87*	99.62	93.6
Stage 5			1.93*	12.1*	49.4*	30.6*
Stage 6				4.2	0.5*	1.4*

Mark-II						
Run	13	15	17	21	19	11
MMD ( $\mu$ )	3.5	1.5	1.5	0.26	0.10	0.049
Stage 1	85.4*	99.26				
Stage 2	<1.0	70.0*	98.6			
Stage 3		0.60*	72.0*	99.84		99.57
Stage 4			8.0*	79.2*	99.15*	98.71
Stage 5			0.84	12.8*	24.6*	78.6*
Stage 6				1.03*	1.7*	3.4*

\* See text.

In Run Nos. 15 and 20, the values less than 1% are also plotted in order to get two points for the corresponding stage. The results of Runs No. 17 and 18 are converted to the standard air flow rate of 8 liters/min by Eq. (6).

The stage constants ( $D_{50}$ ) obtained by this method are plotted versus the stage numbers in Figs. 21 and 22. A deviation between the calculated curve and the experimental one may be noticed for Mark-I. The experimental curve can be described by Eq. (6), if a decreasing impaction parameter is assumed with increasing stage number. This is not the case for Mark-II. All stage constants calculated with an impaction parameter  $\psi = 0.15$  agree with the one calculated.

Based upon this calibration, the stage constants were also calculated for specific gravities other than 1.3 g/cc by Eq. (6). The results are plotted in Figs. 11 and 16.

A photograph of the particle deposition was shown in Fig. 12. It is obviously that the spots differ in intensity. The same phenomenon was discovered by K. R. May<sup>19</sup> with the Andersen Sampler. According to his explanation the stage constants change from the inner holes to the outer ones because of a radial pressure drop. But this means, of course, a superposition of several efficiency curves of different slopes. The resultant is of lower slope and the stage constant is therefore shifted to a higher value. Because of decreasing importance of the radial pressure drop effect<sup>19</sup> with higher stage number and higher total pressure drop across each stage, the deviation of calculated and experimental stage constants becomes smaller at higher stages. Larger clearance between impaction plate and hole plate would reduce the radial pressure drop but lower the slope of the efficiency curve too. In consideration of this known problem, the Mark-II was designed with fewer but larger holes (and therefore larger clearance), and also with a shorter path for exhausted air from the point

of impaction to the next open space. Thus, the radial pressure drop is small and the deposition occurs equally on all spots (Fig. 15). All stages can be described by the same impaction parameter.

#### 8. REFERENCES

1. C. J. Barton, Nuclear Safety 7, 468 (1966).
2. G. W. Parker et al. ORNL-CF-60-12-14 (1960), see also ORNL-NSIC-5.
3. G. W. Parker, H. Buchholz, ORNL-4071, p. 196
4. G. W. Parker, H. Buchholz, ANL Meeting 1967
5. K. R. May, J. Sci. Instr. 22, 187 (1945).
6. W. E. Ranz, J. B. Wong, Ind. Eng. Chem. 44, 1371 (1952).
7. C. N. Davies, M. Aylward, Proc. Phys. Soc. London 64, 889 (1951).
8. A. R. McFarland, H. W. Zeller, TID-18624 (1963).
9. H. Schlichting, Boundary Layer Theory, McGraw-Hill, New York, Chapter 1 (1955).
10. S. C. Stern et al., Ind. Eng. Chem. Fundamentals 1, 273 (1962).
11. R. A. Millikan, Phys. Rev. 22, 1 (1923).
12. T. T. Mercer, LF-12 (1963).
13. G. W. Parker et al. ORNL-4071, pp 52 and 193 (1966).
14. K. T. Whitby et al., Int. J. Air Wat. Poll. Vol. 9, 263 (1965).
15. Andersen Samplers a Consulting Service, 1074 Ash Ave., Provo, Utah, USA.
16. R. I. Mitchell, J. M. Pilcher, TID-7551, p. 67 (1957).
17. J. C. Couchman, CONF-650407 (1965).
18. J. J. Cohen, D. N. Montan, TID-4500 (1966).
19. K. R. May, Appl. Microbiol. 12, 37 (1964).

ORNL-DWG 67-3272

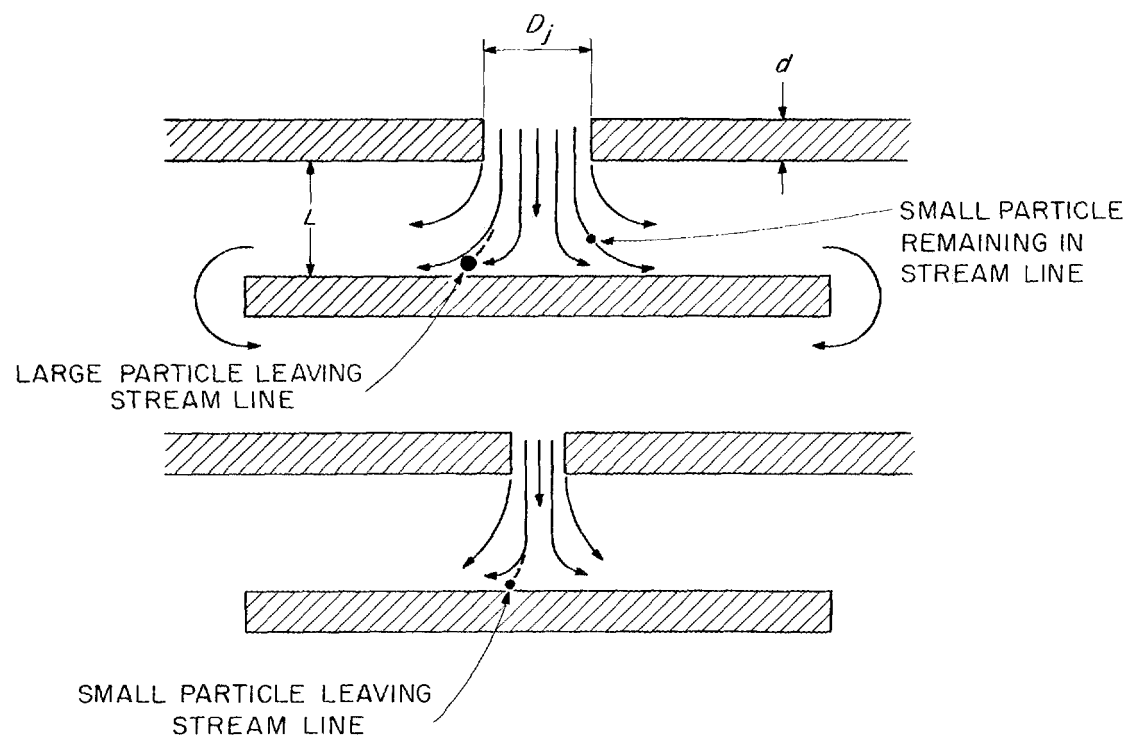


Fig. 1. Impaction Principle

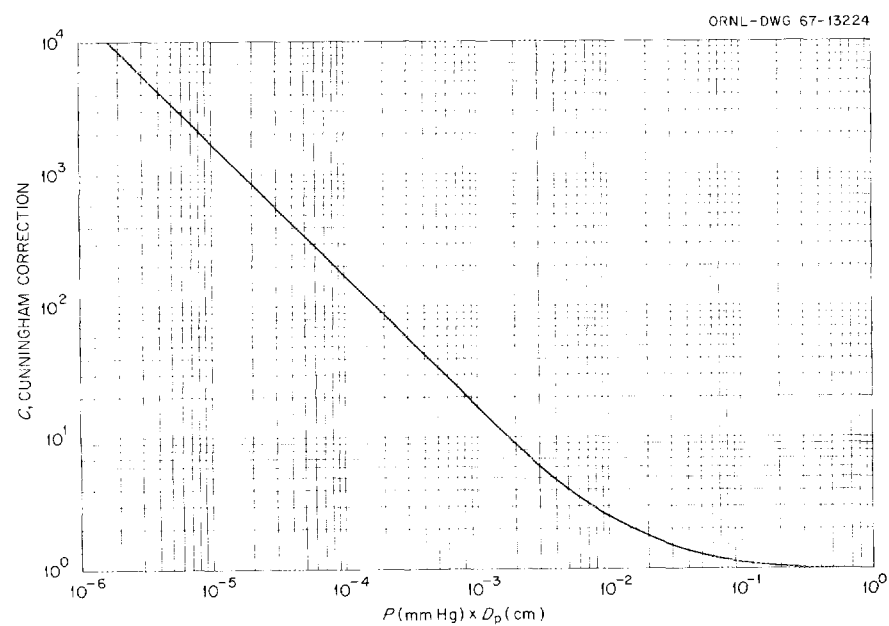


Fig. 2. Cunningham-Correction vs Pressure Times Particle Diameter.

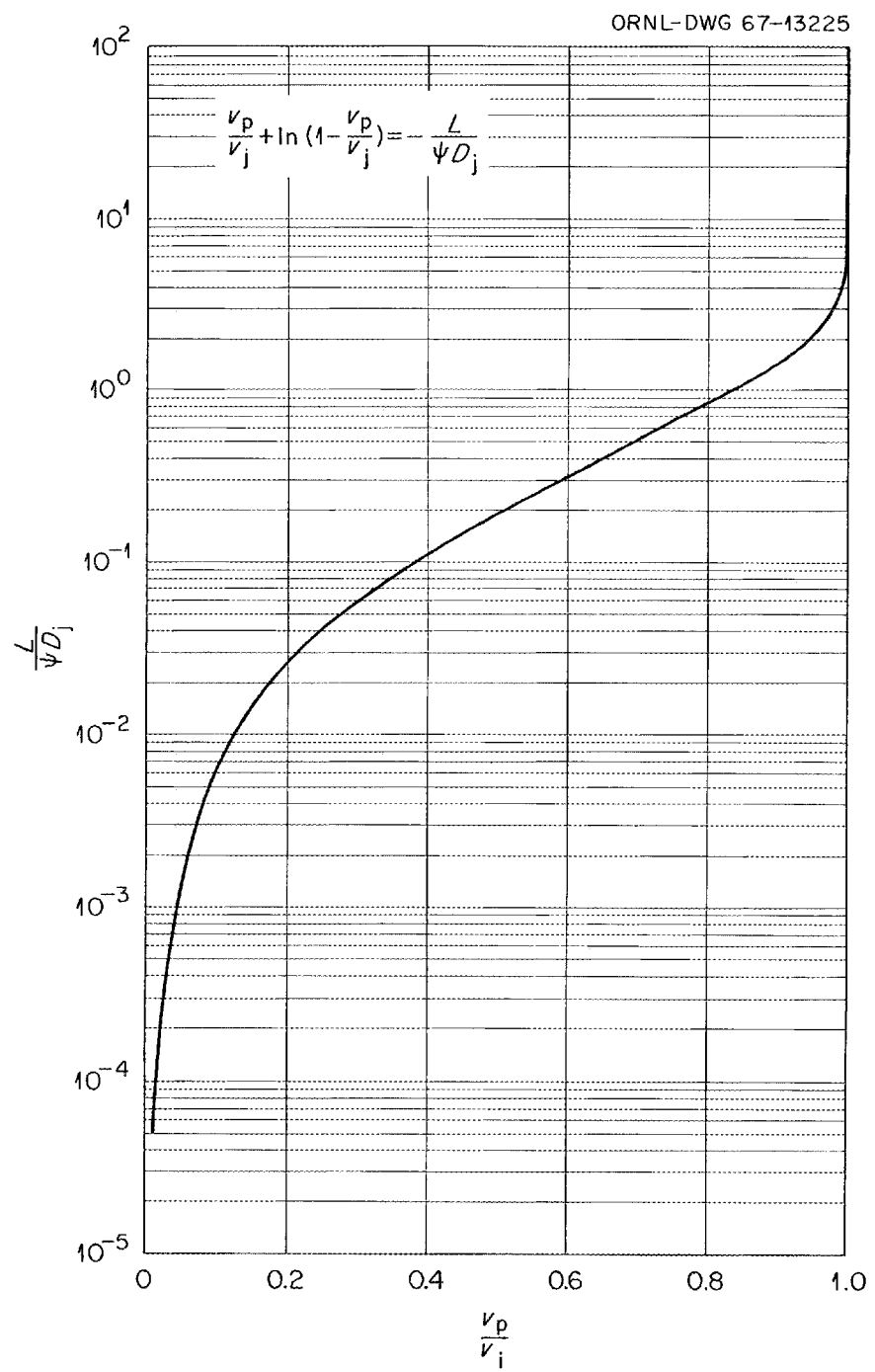


Fig. 3. The Dependence of Relative Particle Velocity on Impaction Parameter.

ORNL-DWG 67-3274R

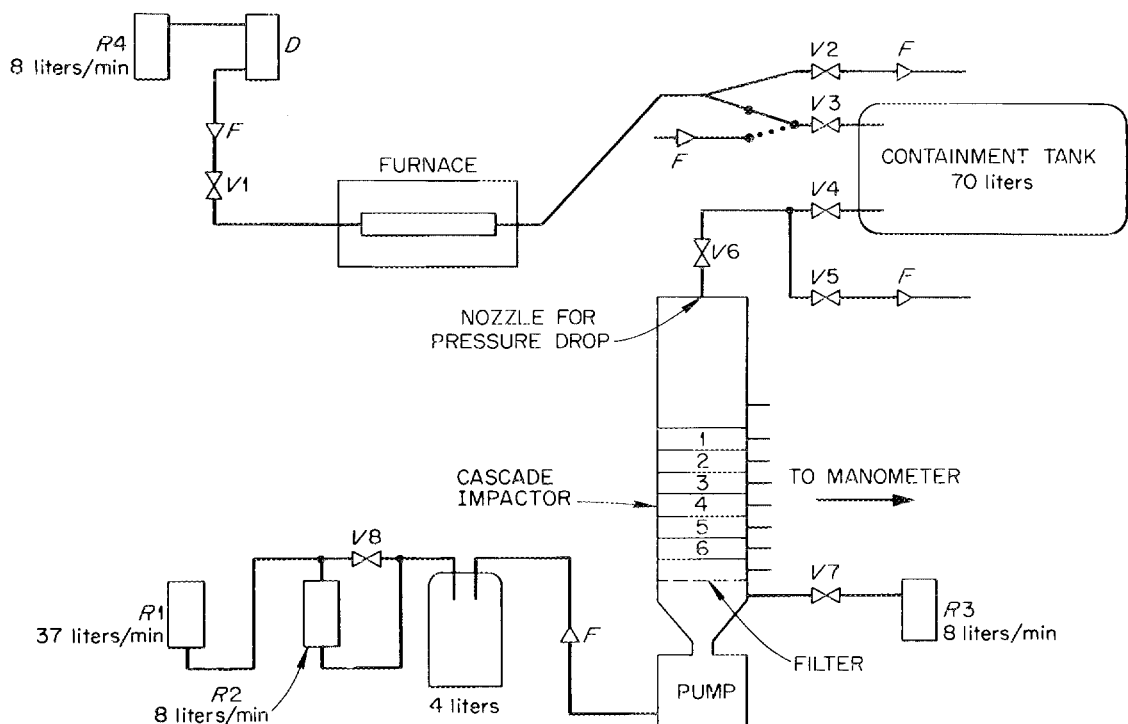


Fig. 4. Schematic Flow Diagram.

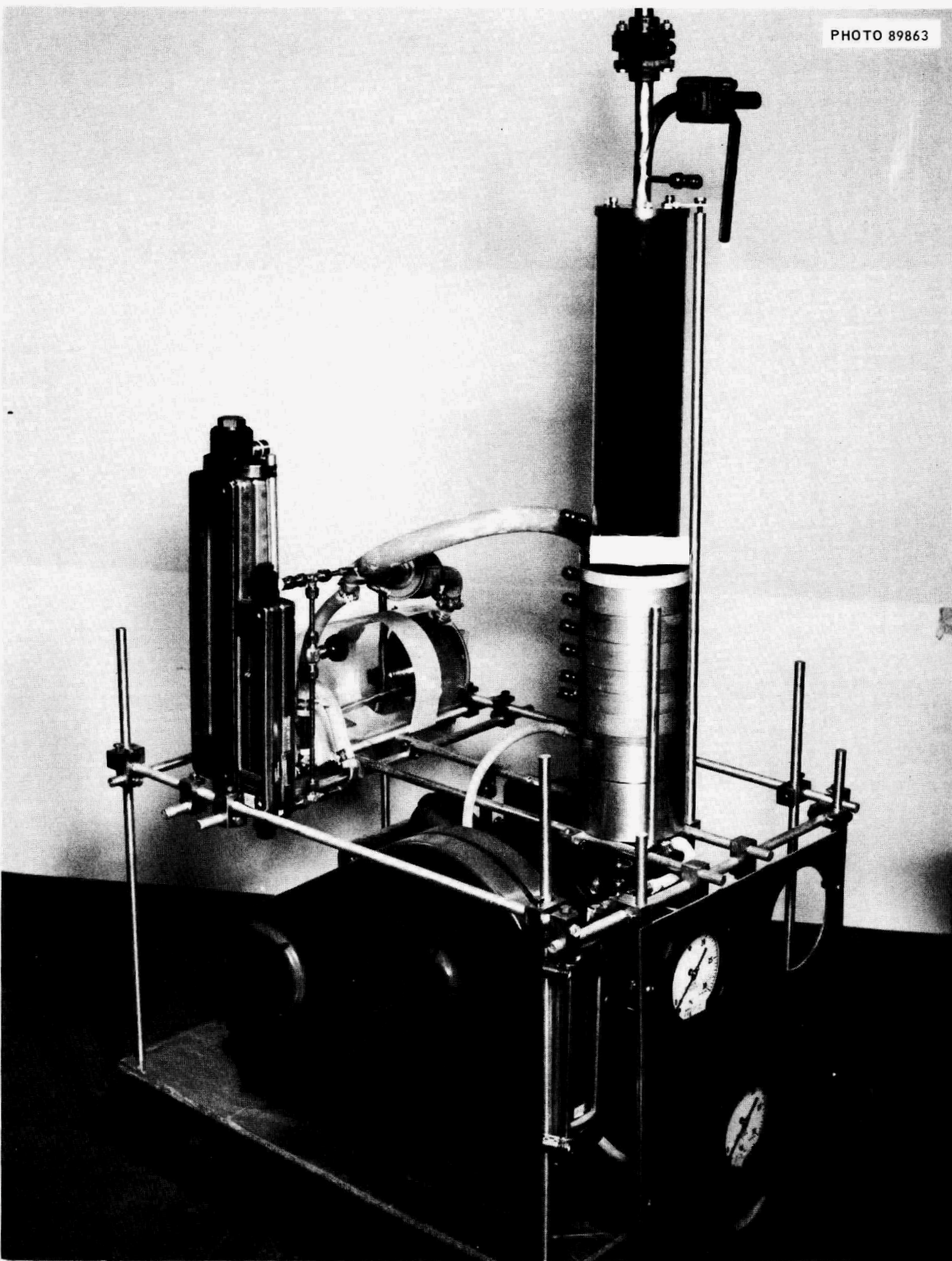


Fig. 5. Impactor Assembly

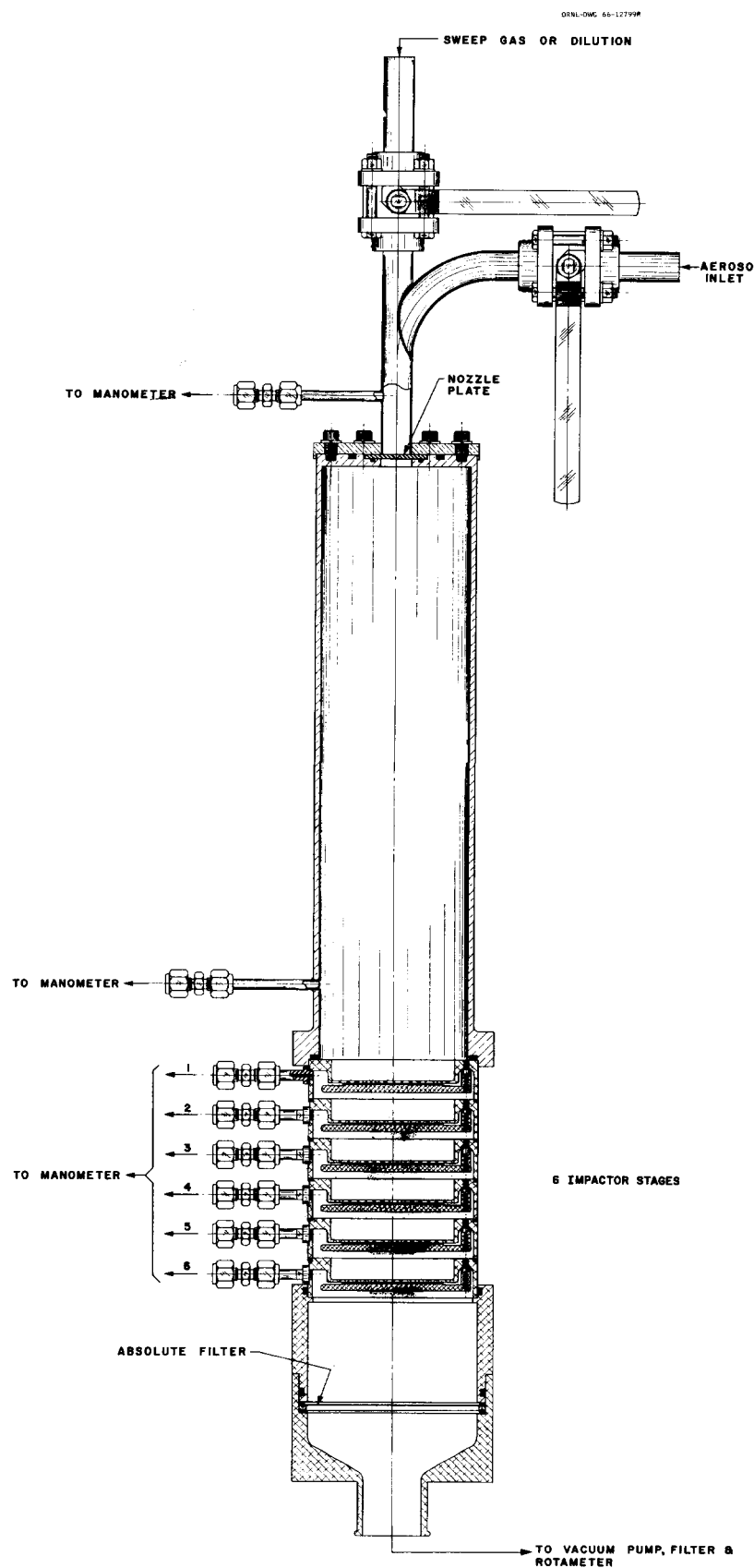


Fig. 6. Low-Pressure Cascade Impactor Mark-I.

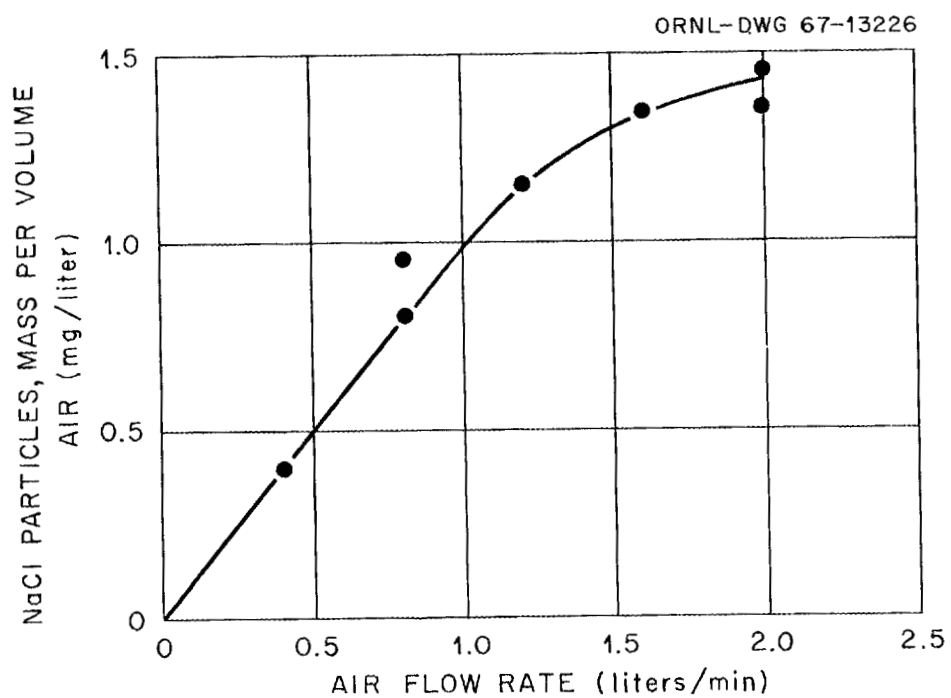


Fig. 7. NaCl Mass Concentration vs Flow Rate  
Downstream of the Furnace.

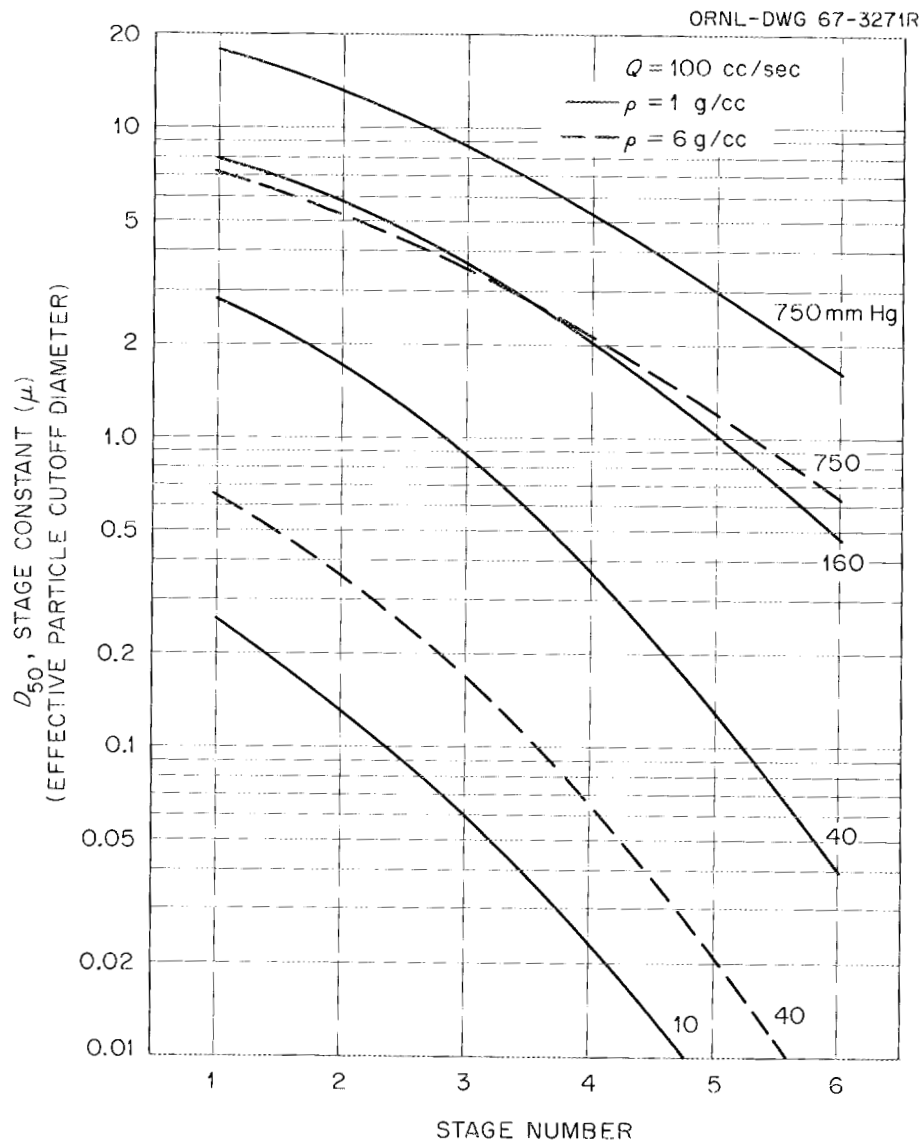


Fig. 8. Calculated Stage Constant Dependence of Andersen Sampler on Pressure and Specific Gravity of Particles.

PHOTO 89397



49

Fig. 9. Low-Pressure Cascade Impactor Mark-I.

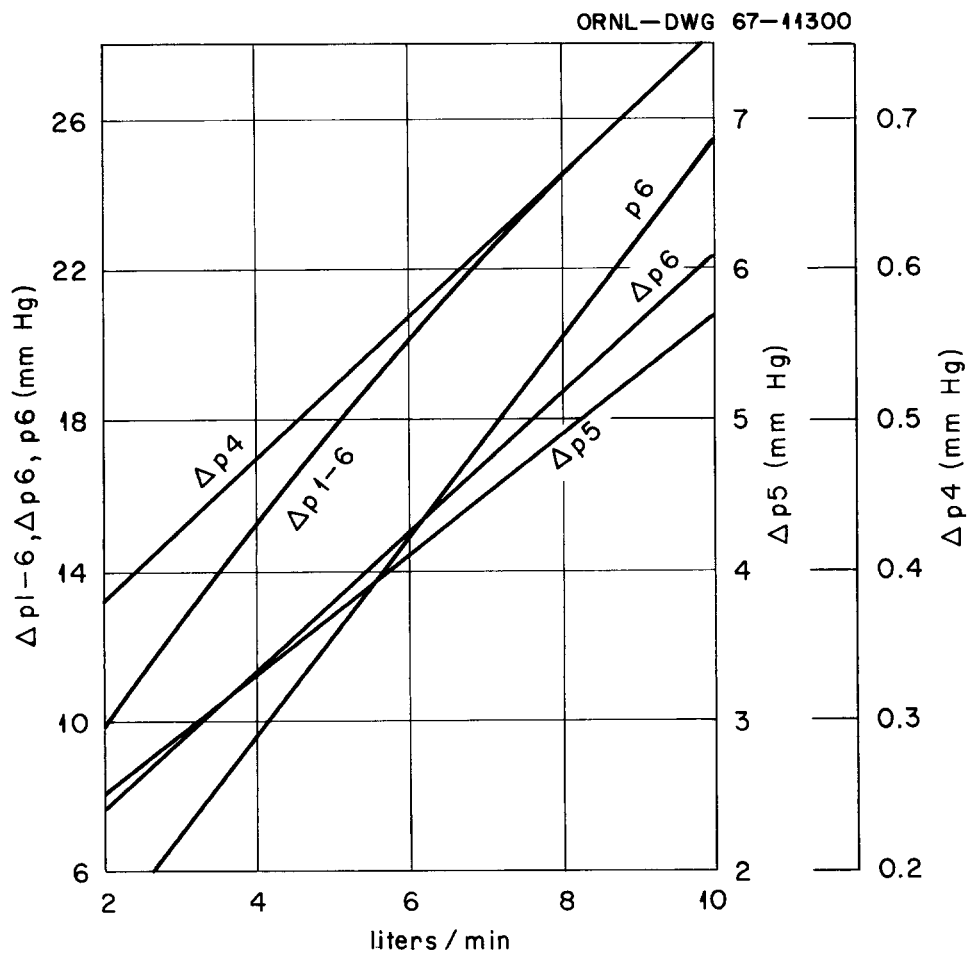


Fig. 10. Pressure and Pressure Drop for Mark-I.

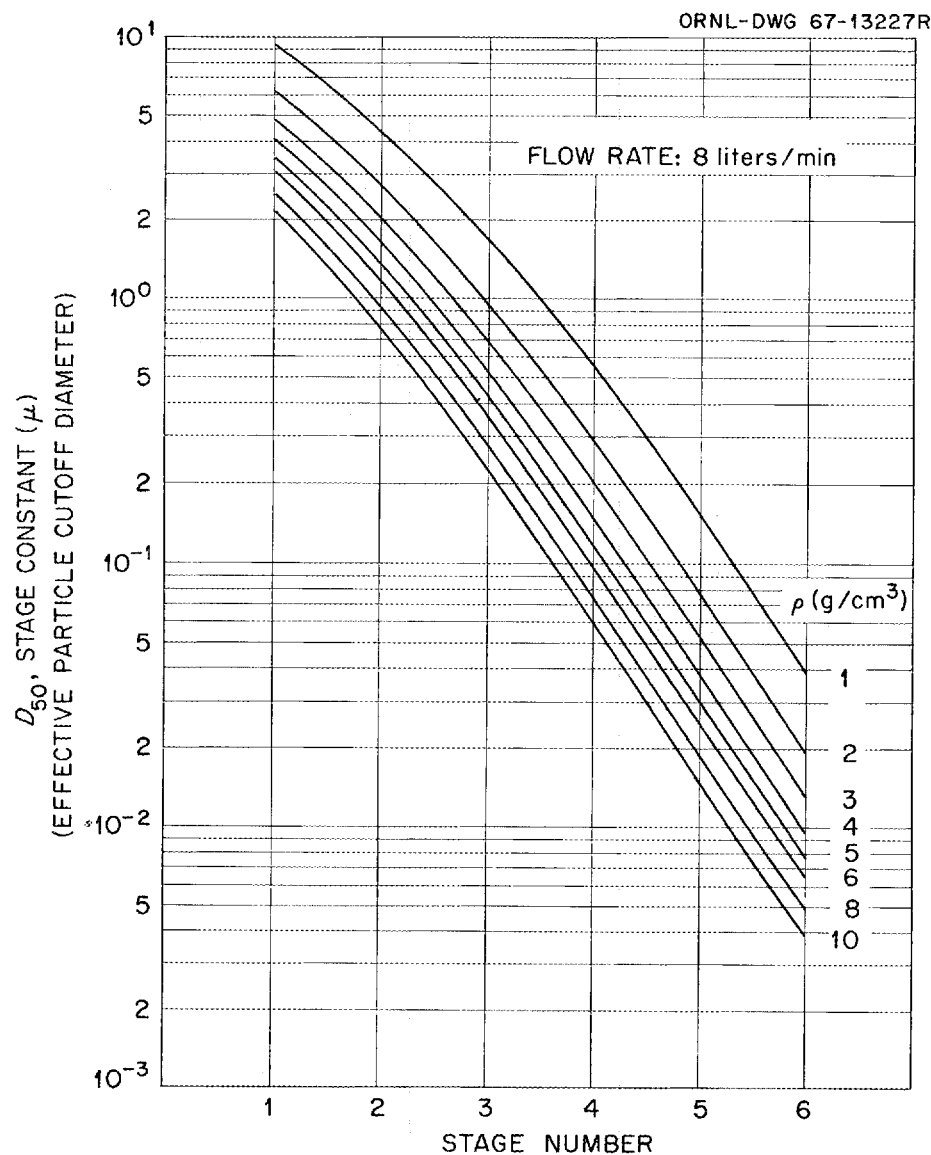
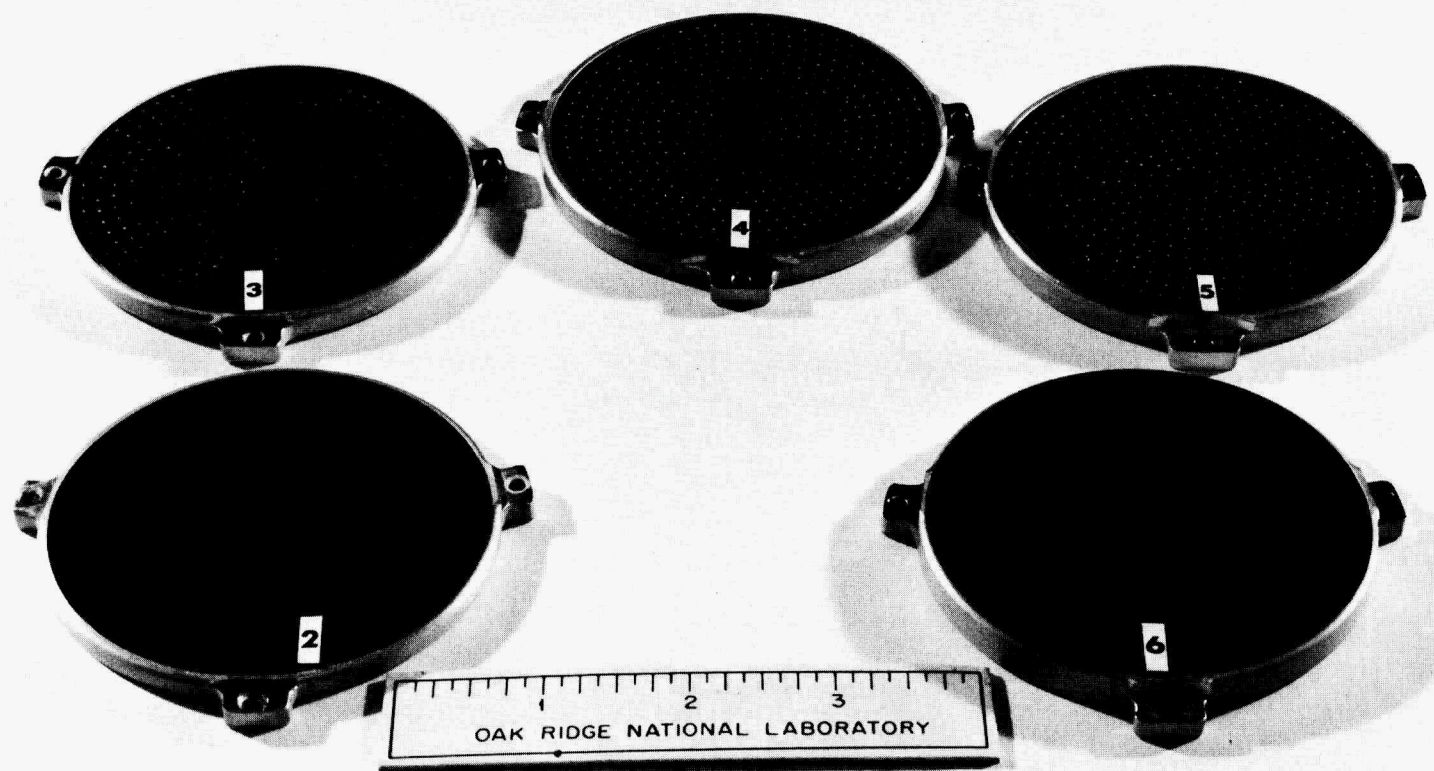


Fig. 11. Calculated Calibration of Mark I Impactor.

PHOTO 89396



52

Fig. 12. Particle Deposition on Mark-I.

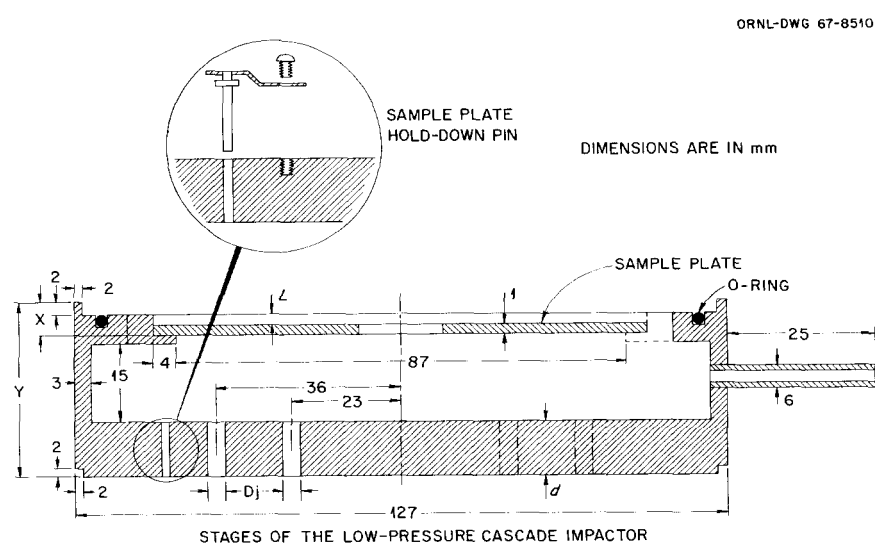


Fig. 13. Design of Mark-II.

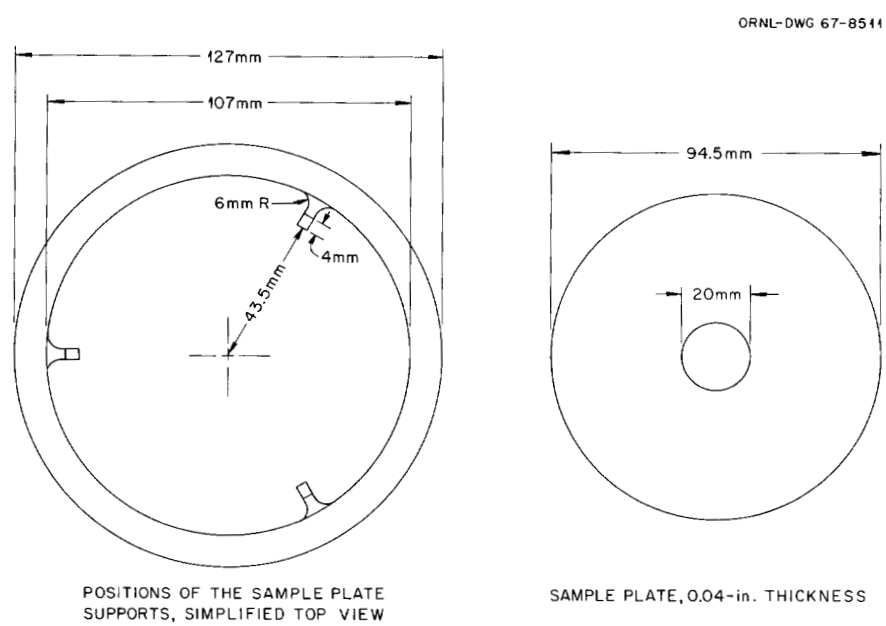


Fig. 14. Design of Mark-II.

PHOTO 89394

55

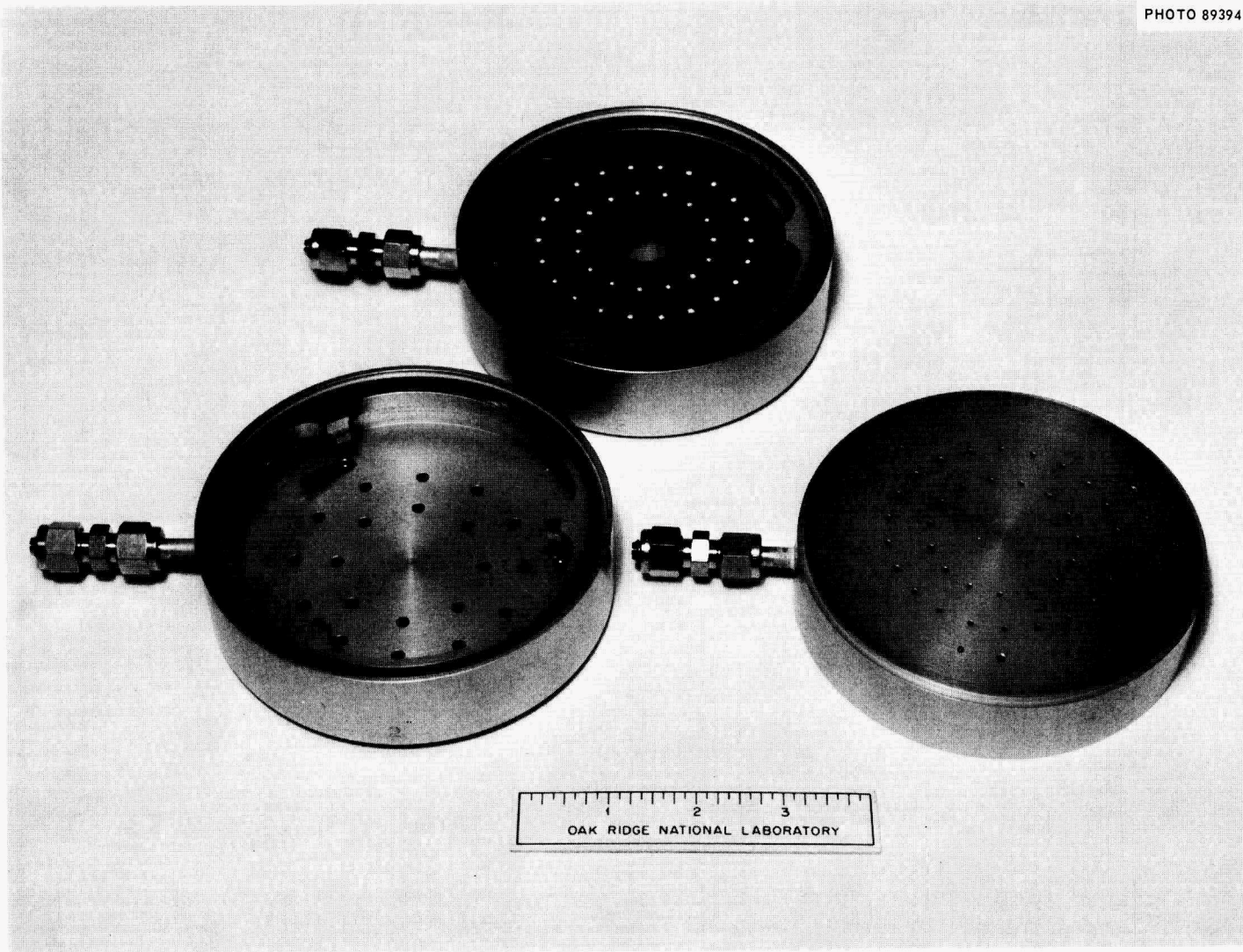


Fig. 15. Low-Pressure Cascade Impactor Mark-II.

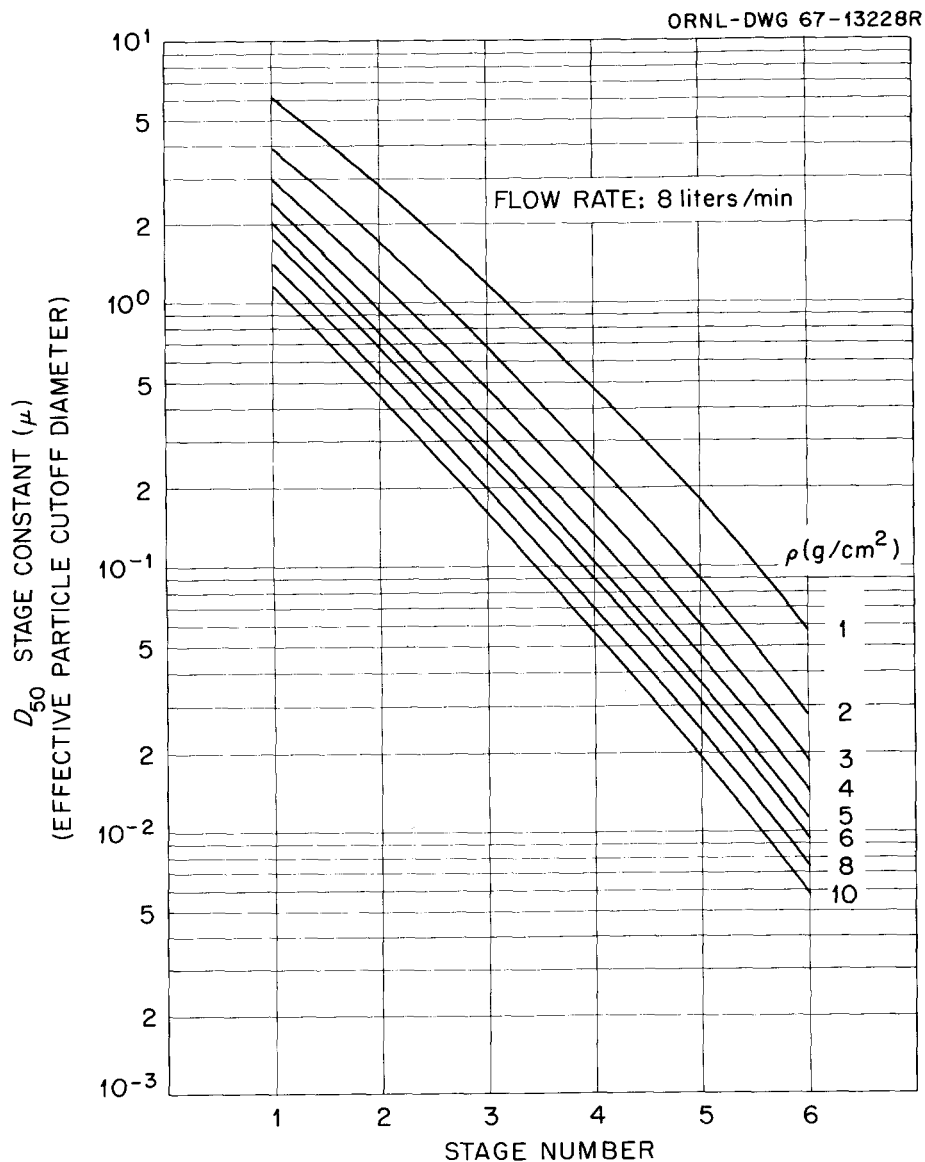
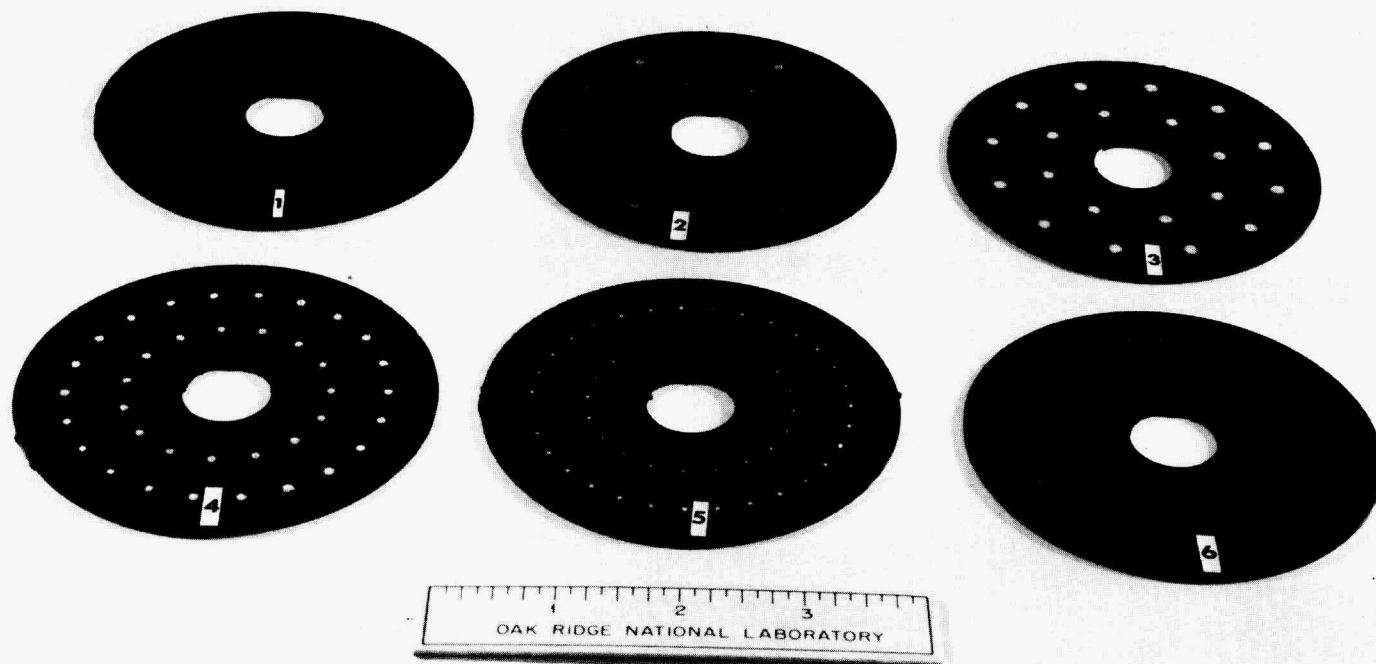


Fig. 16. Calculated Calibration of Mark II Impactor.

PHOTO 89395



57

Fig. 17. Particle Deposition on Mark-II.

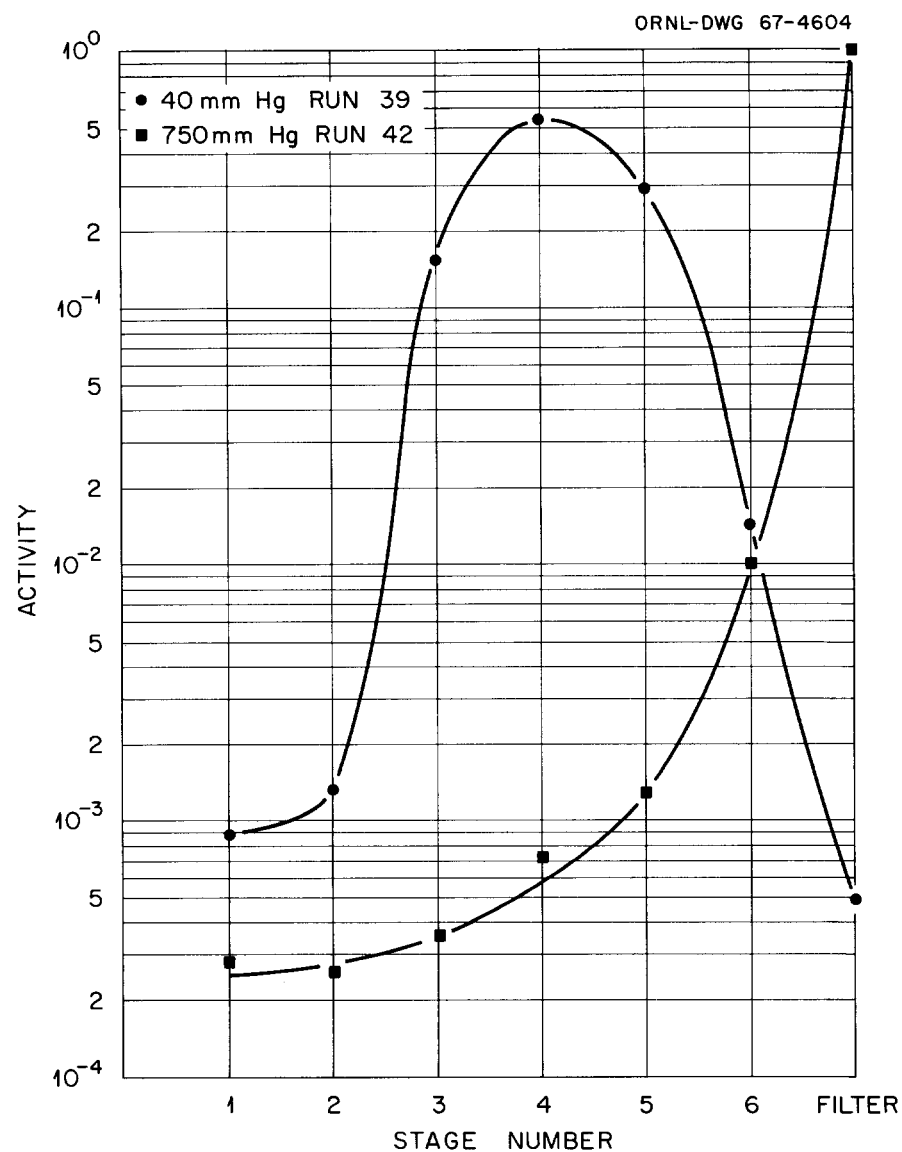


Fig. 18. Fractional Distribution of  $^{134}\text{Cs}$  on Stages and filter at Different Pressures.

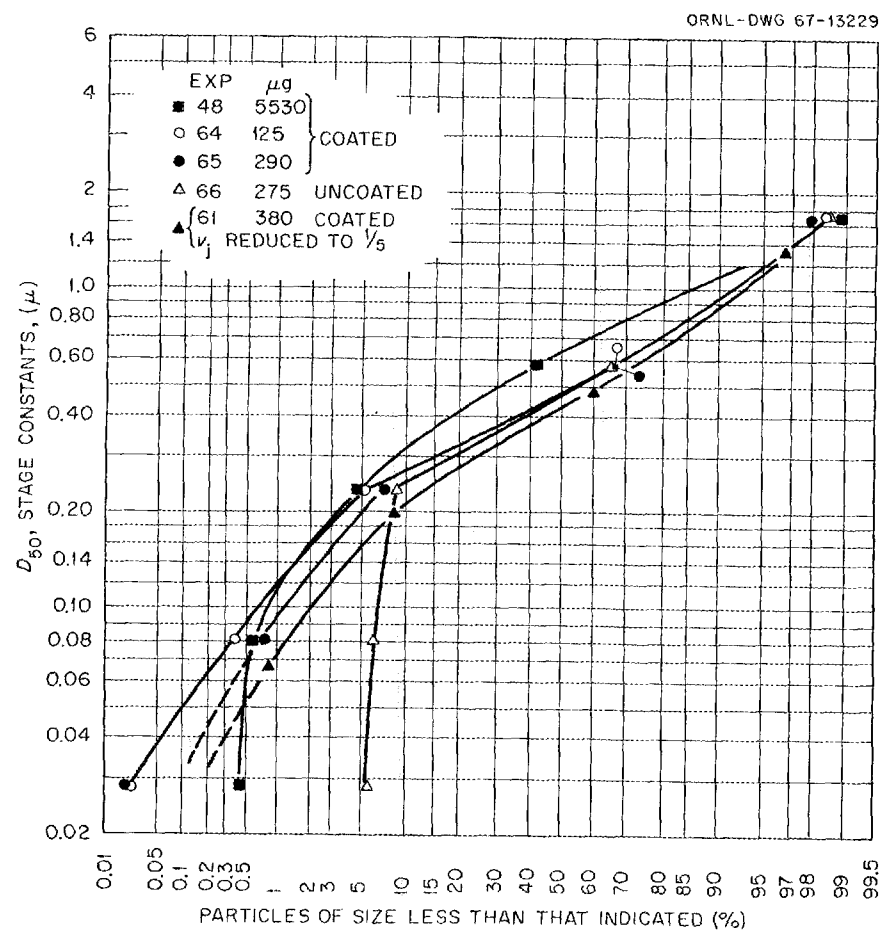


Fig. 19. Stage Constants vs Cumulative Amount of NaCl Deposition in Mark-II Sampler for Different Material Load.

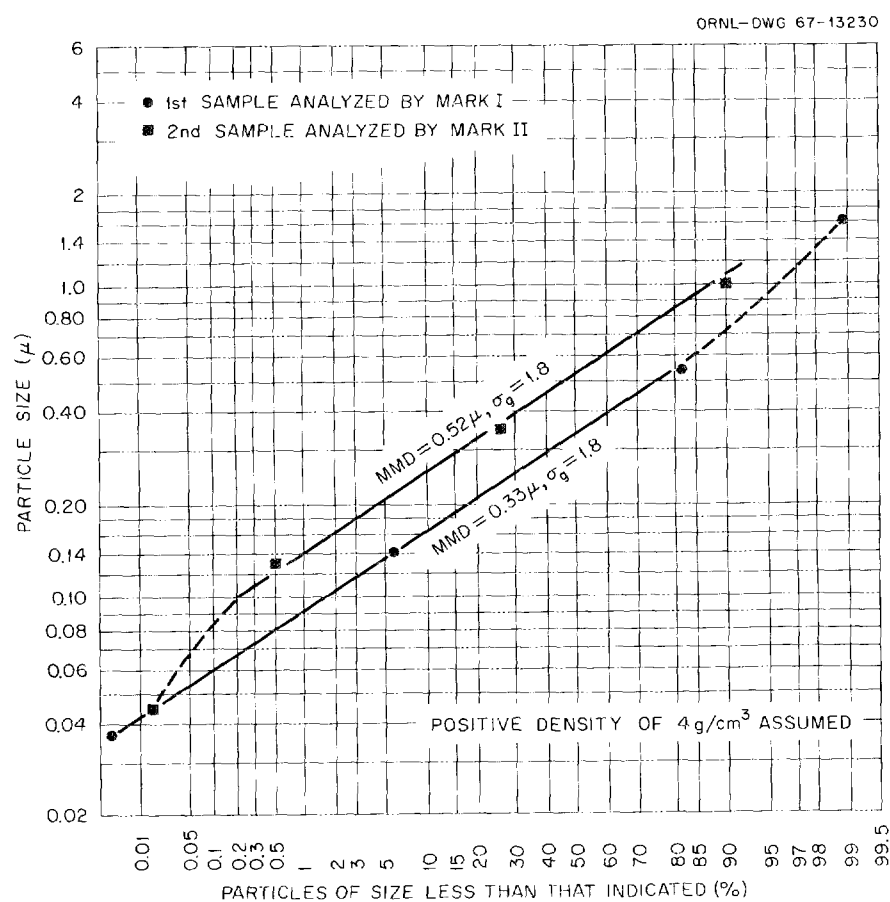


Fig. 20. Size Distribution of Particles Carrying  $^{134}\text{Cs}$ .

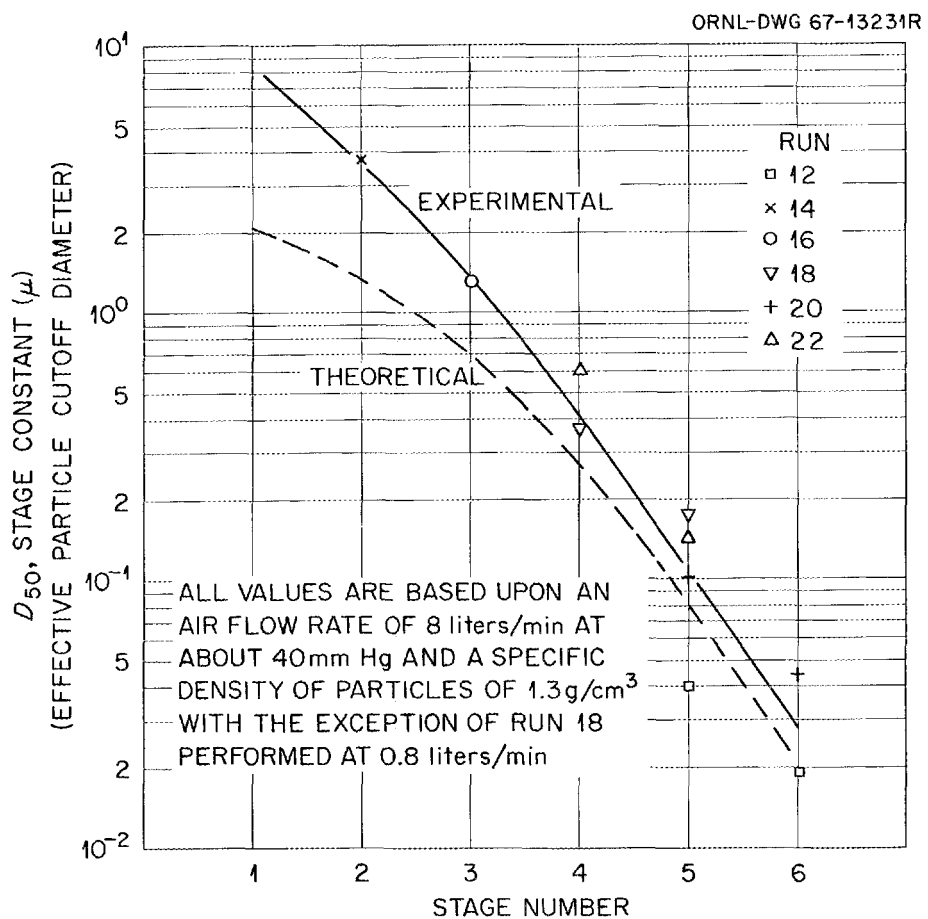


Fig. 21. Calibration of Mark-I Impactor.

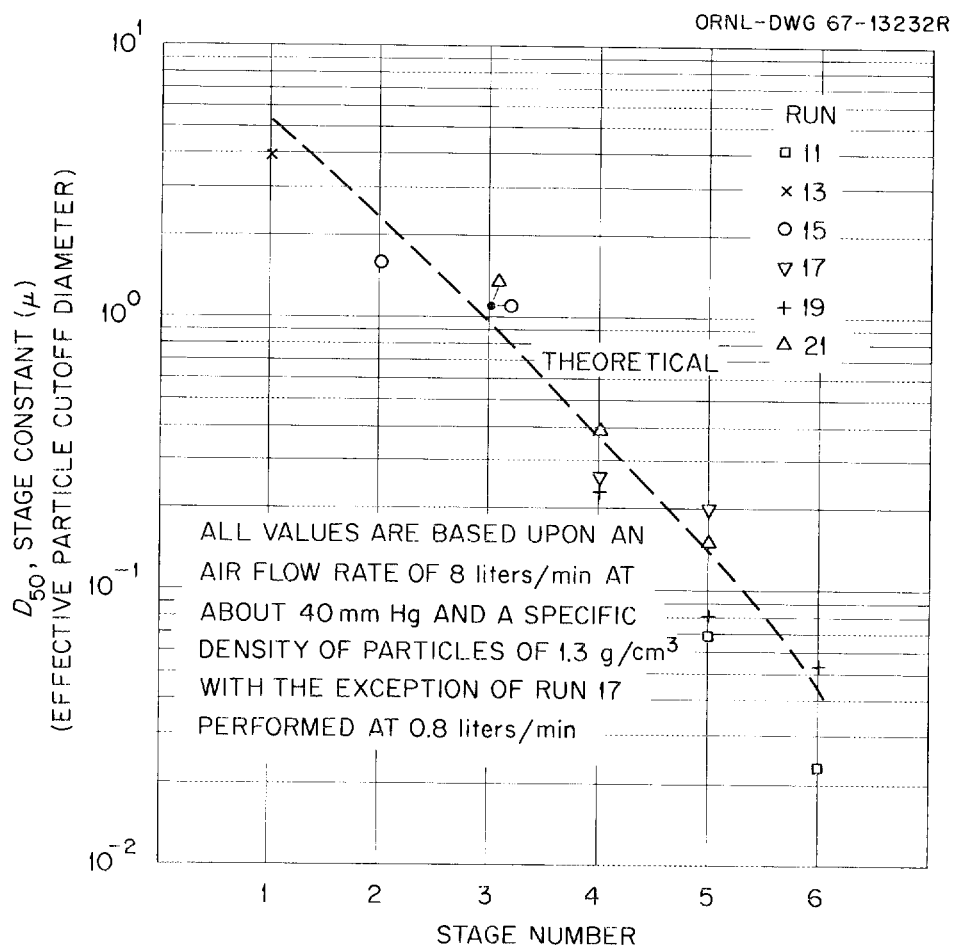


Fig. 22. Calibration of Mark-II Impactor.

ORNL-4226  
UC-80 — Reactor Technology

INTERNAL DISTRIBUTION

- |                                     |                                    |
|-------------------------------------|------------------------------------|
| 1. Biology Library                  | 78. M. M. Martin                   |
| 2-4. Central Research Library       | 79. W. J. Martin                   |
| 5-6. ORNL — Y-12 Technical Library  | 80. W. R. Martin                   |
| Document Reference Section          | 81. H. F. McDuffie                 |
| 7-41. Laboratory Records Department | 82. C. E. Miller, Jr.              |
| 42. Laboratory Records, ORNL R.C.   | 83. F. H. Neill                    |
| 43. R. E. Adams                     | 84-95. G. W. Parker                |
| 44. T. A. Arehart                   | 96. L. F. Parsly, Jr.              |
| 45. W. P. Barthold                  | 97. B. F. Roberts                  |
| 46. F. T. Binford                   | 98. T. H. Row                      |
| 47. E. G. Bohlmann                  | 99. A. F. Rupp                     |
| 48. E. S. Bomar                     | 100. Dunlap Scott                  |
| 49. G. E. Boyd                      | 101. R. P. Shields                 |
| 50. W. E. Browning, Jr.             | 102. O. Sisman                     |
| 51-55. H. Buchholz                  | 103. M. J. Skinner                 |
| 56. T. J. Burnett                   | 104. D. A. Sundberg                |
| 57. C. V. Chester                   | 105. D. B. Trauger                 |
| 58. G. L. Copeland                  | 106. W. E. Unger                   |
| 59-63. W. B. Cottrell               | 107. J. L. Wantland                |
| 64. G. E. Creek                     | 108-112. G. M. Watson              |
| 65. F. L. Culler                    | 113. C. D. Watson                  |
| 66. R. J. Davis                     | 114. A. M. Weinberg                |
| 67. B. R. Fish                      | 115. R. P. Wichner                 |
| 68. M. H. Fontana                   | 116. E. I. Wyatt                   |
| 69. S. H. Freid                     | 117. W. D. Yuille                  |
| 70. W. R. Grimes                    | 118. P. H. Emmett (consultant)     |
| 71. N. R. Horton                    | 119. Norman Hackerman (consultant) |
| 72. J. K. Jones                     | 120. J. L. Margrave (consultant)   |
| 73. G. W. Keilholtz                 | 121. C. R. McCullough (consultant) |
| 74. M. J. Kelly                     | 122. H. Reiss (consultant)         |
| 75. C. E. Larson                    | 123. T. J. Thompson (consultant)   |
| 76. R. A. Lorenz                    | 124. K. T. Whitby (consultant)     |
| 77. H. G. MacPherson                | 125. R. C. Vogel (consultant)      |

EXTERNAL DISTRIBUTION

126. J. A. Swartout, Union Carbide Corporation, New York, N.Y.
127. L. Baker, Argonne National Laboratory, Argonne, Illinois
128. R. E. Baker, Reactor Licensing, U.S. Atomic Energy Commission, Washington, D.C.
129. J. R. Beattie, UKAEA, Risley, England
130. H. Behrman, RDT Site Office, ORNL
131. D. L. Black, Idaho Nuclear, Idaho Falls, Idaho
132. R. Boyd, Reactor Licensing Division, U.S. Atomic Energy Commission, Washington, D.C.
133. W. H. Burgus, Phillips Petroleum Co., Idaho Falls, Idaho

134. A. W. Castleman, Jr., Brookhaven National Laboratory, Upton, N.Y.
135. A. C. Chamberlain, UK-AERE, Harwell, England
136. R. D. Collins, UKAEA, Risley, England
137. D. F. Cope, RDT Site Office, ORNL
138. J. C. Couchman, General Dynamics, Fort Worth, Texas
139. E. Davidson, DRDT, U.S. Atomic Energy Commission, Washington, D.C.
140. R. L. Doan, Regulation, U.S. Atomic Energy Commission, Washington, D.C.
141. F. R. Farmer, UKAEA, Risley, England
142. A. Ferrel, CNEN, Via Belisario 15, Rome, Italy
143. F. A. Gifford, U.S. Weather Bureau, Oak Ridge, Tennessee
- 144-145. H. Gilbert, Division of Operational Safety, U.S. Atomic Energy Commission, Washington, D.C.
146. H. Hamester, DRDT, U.S. Atomic Energy Commission, Washington, D.C.
147. H. Hembree, DRDT, U.S. Atomic Energy Commission, Washington, D.C.
148. R. K. Hilliard, Battelle-Northwest Laboratory, Hanford, Washington
149. W. B. Lewis, AECL, Chalk River, Ontario, Canada
150. J. Lieberman, DRDT, U.S. Atomic Energy Commission, Washington, D.C.
151. G. B. Matheny, Phillips Petroleum Company, Idaho Falls, Idaho
152. F. G. May, UK-AERE, Harwell, England
153. John McAdoo, Westinghouse Atomic Power Division, P.O. Box 355, Pittsburgh, Pennsylvania
154. J. D. McCormack, Battelle-Northwest Laboratory, Hanford, Washington
155. W. J. Megaw, UK-AERE, Harwell, England
156. Tom Mercer, Lovelace Foundation, Albuquerque, New Mexico
157. Peter Morris, AEC, Licensing, Washington, D.C.
158. D. L. Morrison, Battelle Memorial Institute, Columbus, Ohio
159. R. Newton, DRDT, U.S. Atomic Energy Commission, Washington, D.C.
160. I. A. Peltier, AEC, Safety Division, Washington, D.C.
161. J. Pradel, CEA, Fontenay-aux-Roses, France
162. M. E. Remley, Atomics International, Canoga Park, California
163. R. L. Ritzman, Battelle Memorial Institute, Columbus, Ohio
164. C. Sennis, CNEN, Via Belisario 15, Rome, Italy
165. I. Spickler, Reactor Licensing, U.S. Atomic Energy Commission, Washington, D.C.
166. S. Szawlewicz, DRDT, U.S. Atomic Energy Commission, Washington, D.C.
167. D. H. Walker, Phillips Petroleum Company, Idaho Falls, Idaho
168. J. G. Wilhelm, Gesellschaft fur Kernforschung m.b.H, AS-D, Germany
169. T. R. Wilson, Phillips Petroleum Company, Idaho Falls, Idaho
170. R. A. Wiseman, Westinghouse Atomic Power Division, P.O. Box 355, Pittsburgh, Pennsylvania
171. K. Woodward, Reactor Licensing, U.S. Atomic Energy Commission, Washington, D.C.
172. Laboratory and University Division, AEC, ORO
- 173-404. Given distribution as shown in TID-4500 under Reactor Technology category